Biomaterials Advances 188 (2026) 215029

Contents lists available at ScienceDirect

Biomaterials Advances

journal homepage: www.journals.elsevier.com/materials-science-and-engineering-c

Drug-loaded biomorphic scaffolds for tissue regeneration and targeted antitumor therapy in bone metastasis models

Claudia Cocchi [a,1], Valentina Bergamini [b,1], Monica Montesi [c,*], Laura Mercatali [d,**], Massimiliano Dapporto [c], Marta Tavoni [c], Chiara Spadazzi [a], Alessandro De Vita [a], Giacomo Miserocchi [a], Silvia Vanni [a], Giulia Sbanchi [a], Marilisa Cortesi [e,f], Emanuele Giordano [e,g], Roberto Casadei [h], Giacomo Morozzi [i], Alberto Ballardini [i], Ania Naila Guerrieri [d], Enrico Lucarelli [d], Chiara Bellotti [d], Marco Gambarotti [j], Davide Maria Donati [k], Elena Veronesi [b], Massimo Dominici [b,l], Simone Sprio [c], Anna Tampieri [c], Alberto Bongiovanni [m,2], Chiara Liverani [a,2], Toni Ibrahim [d,2]

[a] *Preclinic and Osteoncology Unit, Biosciences Laboratory, IRCCS Istituto Romagnolo per lo Studio dei Tumori (IRST) "Dino Amadori", 47014, Meldola, Italy*
[b] *Technopole "Mario Veronesi", 41037, Mirandola, Italy*
[c] *Institute of Science, Technology and Sustainability for Ceramics (ISSMC), National Research Council (CNR) of Italy, 48018, Faenza, Italy*
[d] *Osteoncology, Bone and Soft Tissue Sarcomas and Innovative Therapies, IRCCS Istituto Ortopedico Rizzoli, 40136, Bologna, Italy*
[e] *Department of Electrical, Electronic and Information Engineering "G. Marconi" (DEI), Alma Mater Studiorum University of Bologna, 47521 Cesena, Italy*
[f] *School of Clinical Medicine, Faculty of Medicine and Health, University of New South Wales, Australia*
[g] *Advanced Research Center on Electronic Systems (ARCES), Alma Mater Studiorum University of Bologna, 47521, Cesena, Italy*
[h] *Orthopaedic and Traumatology Department, "Morgagni-Pierantoni" Hospital, 47121, Forlì, Italy*
[i] *GreenBone Ortho S.p.A., 48018, Faenza, Italy*
[j] *Department of Pathology, IRCCS Istituto Ortopedico Rizzoli, 40136, Bologna, Italy*
[k] *3rd Orthopaedic and Traumatologic Clinic Prevalently Oncologic, IRCCS Istituto Ortopedico Rizzoli, 40136, Bologna, Italy*
[l] *Department of Medical and Surgical Sciences for Children and Adults, University of Modena and Reggio Emilia, Hospital of Modena, 41125, Modena, Italy*
[m] *Departmental Faculty of Medicine, UniCamillus-Saint Camillus International University of Health Sciences, 00131, Roma, Italy*

ARTICLE INFO

Keywords:
Bone metastases
Biomorphic scaffolds
Bone regeneration
Antitumoral treatment
In vitro
In-silico and *ex-vivo* validation

ABSTRACT

Renal cell (RCC) and breast carcinoma (BC) frequently develop lytic bone metastases (BM) that are usually treated with systemic and locoregional therapies. Surgery plays a crucial role when pathological fractures or lesions involve a load-bearing bone and consists in the removal of tumor area followed by replacement with implant or prosthesis. In the present study, a proof of concept of novel locoregional therapies for BM patients was evaluated, consisting in the functionalization of biomorphic apatitic scaffolds with proved intrinsic regenerative properties with Everolimus and an anti-RANKL antibody, selected as relevant anticancer and anti-resorptive biomolecules, respectively. Upon confirmation of the biocompatibility of unloaded scaffolds with healthy bone cells, the effective antitumoral activity of released EVE on BC cell lines (MCF-7 and MDA-MB-231) and RCC cell line (Caki-2) was demonstrated. The inhibitory effects of drugs on osteoclast differentiation were validated using peripheral blood mononuclear cells (PBMCs). Preclinical validation was performed on monocultures and cocultures of cancer and bone cells sharing the same culture medium. *In silico* analyses were exploited to predict cancer cell behavior on medicated scaffolds providing complementary insights while reducing the need for extensive wet-lab experimentation. Finally, as a preliminary proof of translational relevance, the medicated scaffolds were tested with RCC patient-derived explants.

* Correspondence to: M. Montesi, Institute of Science, Technology and Sustainability for Ceramics (ISSMC), National Research Council (CNR) of Italy, Via Granarolo 64, 48018, Faenza, Italy.
** Correspondence to: L. Mercatali, Osteoncology, Bone and Soft Tissue Sarcomas and Innovative Therapies, IRCCS Istituto Ortopedico Rizzoli, Via di Barbiano 1/10, Bologna, Italy.
E-mail addresses: monica.montesi@issmc.cnr.it (M. Montesi), laura.mercatali@ior.it (L. Mercatali).
[1] These authors contributed equally to this work as first authors.
[2] These authors contributed equally to this work as last authors.

https://doi.org/10.1016/j.bioadv.2026.215029
Received 18 February 2026; Received in revised form 14 June 2026; Accepted 17 June 2026
Available online 18 June 2026
2772-9508/© 2026 The Authors. Published by Elsevier B.V. This is an open access article under the CC BY-NC license (http://creativecommons.org/licenses/by-nc/4.0/).

1. Introduction

Bone is one of the most common sites for metastatic dissemination from various cancers, including renal cell carcinoma (RCC) and breast cancer (BC) [1]. Bone relapse negatively affects patients' outcome and quality of life due to skeletal-related events (SREs), including pathological fractures, spinal cord compression, radiation to the bone for pain, surgery to the bone for stabilization and hypercalcemia [2]. For BC patients, the median survival following a diagnosis of bone metastasis (BM) is between three and five years [3]. For patients with RCC, the prognosis is quite heterogeneous ranging from 19 to 31 months depending on several factors [4–6].

Patients with BM can benefit from integrated treatment approaches, including systemic therapies and bone-targeted agents (BTA). Everolimus (EVE), an inhibitor of the mTOR pathway, is indicated for patients with metastatic RCC and hormone receptor-positive BC [7,8]. The mTOR pathway is also involved in the process of osteoclastogenesis, therefore the use of EVE in BM setting could simultaneously exert antitumoral effects on cancer cells and inhibit bone resorption, thereby promoting bone regeneration [8,9]. On the other hand, the two most often utilized BTAs are the monoclonal antibody anti-RANKL (Receptor Activator of Nuclear Factor Kappa-B Ligand), commercial name Denosumab, and zoledronic acid. Both drugs disrupt the vicious cycle that occurs between cancer and resident cells at the bone metastatic site [10]. Specifically, cancer cells begin expressing RANKL and stimulate osteoblasts (OBs) to produce RANKL with a resulting increase in the maturation of bone degrading osteoclasts (OCs). Bone resorption, in turns, promotes the release of growth factors that are necessary to sustain cancer cell colonization and proliferation [11]. Denosumab has been demonstrated to be usually well tolerated and more effective than zoledronic acid in preventing SREs from BC, prostate cancer, and other advanced solid tumors including RCC [12,13]. Denosumab can successfully decrease the risk of clinical fracture and reduce bone loss due to treatments with mixed results in terms of disease-free survival (DFS) in hormone receptor positive/her2-negative BC patients receiving aromatase inhibitor therapy [14].

Besides these medical interventions, depending on the fracture risk, BC and RCC-derived BMs can be treated surgically [15], providing the removal of metastatic tissue and replacement of the excised bone with prostheses or bioimplants [16]. The surgery is often performed with palliative intent to improve patients' quality of life. However, in specific situations - such as single lesions, lesions in load-bearing bones, or cases with a high risk of pathological fracture - surgery may also have a curative purpose, with the metastatic tissue being replaced with a bone substitute [17,18]. This comprehensive strategy not only eliminates cancer cells but also promotes bone regeneration. Synthetic implants, which may be composed of metallic (usually, titanium alloys and stainless steel) [19], polymeric (usually, ultra-high molecular weight poly-ethene) [20] and/or ceramic (usually, zirconia or alumina) materials are chosen for metastatic bone reconstruction due to their ability to allow for early weight-bearing and mobility [21]. However, the majority of bone graft alternatives like synthetic bioactive cements and ceramics, including most of calcium phosphate-based scaffolds which, even though widely recognized as golden standard for bone regeneration due to their biocompatibility and osteoconductivity, lack of significant osteoinductivity. The reason is that the manufacturing process uses high temperatures, which reduce the bioactivity and bioresorbability typical of nanostructured apatitic phases [22–24]. Moreover, without other complementary treatments (like radiotherapy and systemic antitumor therapies), different degrees of tumor progression and detrimental bone instability may occur in metastatic sites [25]. An intralesional resection also entails the risk of spreading the tumor cells, which may result in new lesions developing in the surrounding tissues. Recent advances in bone tissue engineering have opened new avenues for bone repair and treatment after surgery for BM. To reduce the risk of local recurrence, some studies suggested adding chemotherapeutic agents to bone implants as complementary local treatment [26–29]. Controlled drug release by medicated scaffolds has a great relevance for medical applications; however, this approach is still limited by the difficulty in tuning the amount of released drug within the therapeutic range avoiding any harmful effects [30].

In the present study, we developed bioactive 3D apatitic scaffolds functionalized with EVE and an anti-RANKL antibody, with the purpose to generate a proof of concept of novel locoregional therapies for BM patients, pinning on a combination of the scaffold regenerative ability and the antitumoral function of the loaded drugs. The scaffolds were obtained by a recently developed biomorphic transformation which is a sinter-free process, starting from natural rattan wood and yielding 3D nanostructured Mg^{2+}/Sr^{2+}-doped hydroxyapatite (HA), retaining the original hierarchical wood structure, which closely mimics the osteon architecture of compact bone [31]. Such unique features favor the regulation of stem cells' fate and the crosstalk between mesenchymal stem cells (MSCs) and endothelial cells towards effective bone and vascular development, as shown by recent *in vitro* and *in vivo* tests [31–33]. In addition, the hierarchical porous structure of this material enables damage-tolerant mechanical behavior, unusual for a pure ceramic material [31–34], mimicking the healthy bone tissue, very relevant to re-establish its physiological biomechanics [35]. We analyzed the drug release profile and the potential ability of medicated biomorphic apatitic scaffolds to exert tumor killing and regenerative effects at the same time, by applying preclinical *in vitro*, *ex vivo* and *in silico* models of BM from BC and RCC.

2. Materials and methods

2.1. Preparation of biomorphic scaffolds

Pieces of rattan wood (*Calamus manna*) were used as 3D templates and shaped to form a cylinder with a final diameter of 10 mm. The wood was then heated to 900 °C (heating/cooling rate: 1 °C per minute) in a nitrogen atmosphere to remove the organic components and produce a carbon template. This carbon template was placed in a vessel with metallic calcium granules (Sigma Aldrich, United States) and heated to 1200 °C (heating/cooling rate: 2 °C per minute) in a vacuum furnace under an argon atmosphere (pressure: 100 mbar), allowing calcium sublimation. The resulting CaC_2 template was then transformed into CaO by heating it to 1100 °C in air. Further, CaO was converted to $CaCO_3$ by heating under CO_2 pressure at 100 atm, from room temperature to 800 °C, under non-isothermal and isobaric conditions. This was done in wet conditions using hydrated CO_2 with a CO_2/H_2O molar ratio of 8 to 10. During this step, CO_2 remained in its supercritical state, enabling the reaction. Next, the resulting $CaCO_3$ structure was immersed in a 3.0 M solution of $(NH_4)2HPO_4$ (Sigma Aldrich, United States) at pH 8.5 and heated to 220 °C under water vapor pressure (~20 bar) to initiate a dissolution-reprecipitation reaction, converting $CaCO_3$ to calcium phosphate. The material was then treated in an aqueous solution containing 0.5 M $SrCl_2$ and 0.5 M $MgCl_2$ at 50 °C for 24 h at pH 7.0, resulting in a biphasic biomorphic apatite scaffold composed of HA and β-tricalcium phosphate (β-TCP) doped with Mg^{2+}, Sr^{2+}, and CO_3^{2-} ions. Finally, the 10 mm diameter cylinders were cut into discs of 3 mm and 4 mm in height and sterilized using gamma radiation for *in vitro* tests. This method mirrors the process used in producing b.Bone, as described by Sprio et al. [36] and Salamanna et al. [37]. Prior to cell seeding, biomorphic scaffolds underwent gamma radiation sterilization and were then pre-conditioned for 72 h with 5 mL of culture media at 37 °C, 5% CO_2.

2.2. Characterization of biomorphic scaffolds

Biphasic calcium phosphate granules were coated with gold using a Desk V Sputter (Denton Vacuum) for surface topography analysis. Their surface was examined by scanning electron microscopy (SEM) using a

Thermo Fisher Scientific Phenom XLG2, operated at an acceleration voltage of 15 keV and 30 mA.

2.2.1. X-ray diffraction (XRD)

The XRD patterns were recorded using Cu Kα radiation (λ = 1.5417 Å) generated at 40 kV and 40 mA as the X-ray source on a D8 Advance diffractometer (Bruker, Karlsruhe, Germany) equipped with a Lynx eye position sensitive detector. Spectra were recorded with a step size (2θ) of 0.02 and a counting time of 0.5 s in the 2θ range 10–80°, referring to JCPDS 09–0432 and 09–0169 for HA and β-TCP, respectively.

2.2.2. Fourier-transformation infrared spectroscopy (FT-IR)

The FT-IR analyses were performed in the range 4000 to 400 cm^{-1} with a Nicolet iS5 spectrometer (Thermo Fisher Scientific Inc., Waltham, MA, USA), using a resolution of 2 cm^{-1}.

2.2.3. Inductively coupled plasma optical emission spectroscopy (ICP-OES)

The chemical composition of the specimens was assessed with an Agilent 5100 ICP-OES spectrometer (Agilent Technologies, Santa Clara, CA, USA). In particular, 20 mg of powder was dissolved in 2 wt% HNO_3 solution. Standard solutions of the analyzed element (Ca, P, Mg, Sr), obtained by dilution of certified 1000 ppm standards (Sigma Aldrich, St. Louis, MO, USA) were used to obtain the calibration curve in the concentration range 1–100 ppm.

2.2.4. Porosity

The total porosity of the samples has been calculated using the formula $P = [1-(d_c/d_{th})]*100$ where P is the porosity percentage, d_c is the density (calculated) and d_{th} is the density (theoretical).

The microstructure of the samples was assessed by SEM using a field emission microscope (FE-SEM, mod. ΣIGMA, ZEISS NTS GmbH, Oberkochen, Germany) with a 4.00 kV operating voltage.

2.2.5. UV–Visible spectrophotometer

The absorption kinetics and the release profiles of EVE was investigated by UV–visible spectroscopy (LAMBDA™ 750 UV/Vis/NIR spectrophotometer from PerkinElmer).

2.2.6. High-performance liquid chromatography

The quantification of anti-RANKL by High-Performance Liquid Chromatography (HPLC) was carried out using a 1260 Infinity II LC System (Agilent Technologies, Santa Clara, USA). Analyses were performed using an Agilent Eclipse Plus C4 column (100 mm × 2.1 mm, 3.5 μm, Agilent Technologies, Santa Clara, USA). The mobile phase was a mixture of 75:25% *v*/v of an aqueous solution of 30 mM Na_2SO_4 and ACN with TFA (0.05% *v*/v). The sample was eluted at a flow rate of 1.0 mL/min, the temperature was set at 25 °C and the wavelength for the anti-RANKL antibody detection was fixed at 214 nm. The elution time of the anti-RANKL antibody was 10.4 min.

2.3. Drug-loaded protocols for medicated scaffolds

EVE (SML2282, Sigma Aldrich, St. Louis, MO, USA) was dispersed in DMSO (2 mg/mL). To obtain the two requested released concentrations of 0.1 μg/mL and 0.05 μg/mL, respectively corresponding to the plasma peak and half of the plasma peak concentration, two different drug solutions were prepared in DMSO at 200 μg/mL and 100 μg/mL. Then, 100 μL of these solutions were separately dispensed on each specimen, resulting in the final functionalization of the scaffolds with 20 μg and 10 μg of EVE, respectively. The anti-RANKL antibody solutions were prepared at 10 mg/mL in water. Then, 50 μL of the solutions were separately dispensed on each specimen, resulting in the functionalization of the scaffolds with 500 μg. The medicated scaffolds were pre-conditioned in culture medium for 24 h to allow for the initial burst release.

2.4. Evaluation of drug release

EVE release tests were performed after the DMSO evaporation at room temperature in solvent hood (≈2 h). Then, the samples were immersed in 5 mL of HEPES solution (0.01 M, with KCl 0.01 M, pH 7.4) and stored in a thermostatic stirrer in dark condition at 37 °C for up to 14 days. At each time-point, the whole volume of HEPES solution was freeze-dried, dispersed in 0.5 mL of DMSO solution and analyzed by UV–visible spectroscopy.

The anti-RANKL antibody release experiment was conducted after water evaporation in the solvent hood (≈2 h). Samples were immersed in 5 mL of HEPES solution (0.01 M with KCl 0.01 M, pH 7.4) in a thermostatic stirrer in dark condition at 37 °C for up to 7 days. At each timepoint 50 μL of HEPES solution was collected and renewed with the same volume and analyzed by HPLC.

2.5. In vitro culturing of cancer cells

The experiments were performed on MCF-7 and MDA-MB-231, which are estrogen receptor-positive and triple negative BC cells (TNBC), respectively, and on Caki-2, a human clear-cell renal carcinoma cell line (ccRCC). All cell lines were purchased from the American Type Culture Collection (ATCC, Rockville, MD, USA). Cancer cells were maintained as a monolayer in 75 cm^2 flasks at 37 °C in α-MEM (LONZA, Basel, Switzerland) supplemented with 1% glutamine (PAA), 1% Penicillin/Streptomycin, and 10% fetal bovine serum (FBS) in a 5% CO_2 atmosphere (complete α-MEM). Cancer cells were cultured at a density of 5×10^4 cells on biomorphic scaffolds or in 24-well plates in monolayer conditions. Cells were seeded onto the scaffolds as a suspension in 30 μL of culture medium, applied in small droplets, and incubated for 1 h at 37 °C to allow for cell attachment. Viability was analyzed by MTT assay (Sigma Aldrich, according to manufacturing protocol) at different time points (24 h, 72 h and on day 7) to obtain a growth profile over time.

2.6. Osteoclasts differentiation from human peripheral blood mononuclear cells and THP-1 cell line

Peripheral blood mononuclear cells (PBMCs) were isolated from buffy coats of healthy donors who gave written informed consent to take part in the study, by Ficoll density gradient as described in Mercatali et al. [9]. Briefly, fifty mL of EDTA-treated whole blood (50 mL) was diluted 1:1 with Phosphate buffered saline (PBS 1×), layered on lymphocyte separation media (Lymphosep, Biowest, Nuaillé, France) and centrifuged without brakes at 1000 ×*g* for 10 min. PBMCs were collected and washed twice with PBS 1× and resuspended in complete α-MEM. The conditions to differentiate OCs on standard monolayer were already established [9]. Cells were plated in monolayers, at a concentration of 1.5×10^6 PBMCs in the 24-well plate and, after 4 h of attachment at 37 °C, the medium was removed and osteoclastogenesis was induced by adding complete α-MEM supplemented with 20 ng/mL of Monocyte colony stimulating factor (M-CSF) (Cod. 300–25; Peprotech, Rocky Hill, NJ, USA). For the biomorphic scaffold, the seeding concentrations tested were 1.5×10^6 and 3×10^6 cells and performed as previously reported. From day 7 of culture, 20 ng/mL of RANKL (Cod. 310–01; Peprotech, Rocky Hill, NJ, USA) was added with M-CSF. The medium was changed every 3 days. At the end of experiments, after 14 days, cells were fixed by incubation in 4% Paraformaldehyde (PFA - Cod. 157–4; Polyscience, Niles, IL, USA) for 15 min at room temperature.

The human monocytic cell line THP-1, purchased from ATCC (Manassas, VA, USA), was also employed. Cells were cultured in α-MEM (Gibco, Thermo Fisher Scientific, Waltham, MA, USA), supplemented with 10% fetal bovine serum (FBS, Euroclone, Pero, MI, Italy), 1% Penicillin/Streptomycin (Gibco, Thermo Fisher Scientific, Waltham, MA, USA), and 2% L-Glutamine (Gibco), to support cell growth and viability. Cell cultures were maintained at a density of 8×10^5 cells/mL

in standard incubator conditions (37 °C, 5% CO_2). THP-1 differentiation into mature OCs was performed by addition of M-CSF and RANKL (Sigma-Aldrich, Merck KGaA, Darmstadt, Germany), at a final concentration of 25 ng/mL.

2.7. Osteoblasts differentiation from hMSCs

Human mesenchymal stem cells (hMSCs; Cat. SCC036; derived from human embryonic stem cells - Merck Millipore) were seeded in monolayer at a density of 3×10^3 cells/cm^2, and on biomorphic scaffolds at a density of 5×10^4 cells, as previously described [38]. The osteogenic medium was composed of complete α-MEM, Dexamethasone 100 nM, β-glycerophosphate 10 mM, ascorbic acid 200 μM and Bone Morphogenetic Protein-2 (BMP-2) 100 ng/mL as differentiation factors. The medium was changed every 3 days. After 14 days, cells were fixed in 4% PFA for 15 min.

2.8. Osteoblasts differentiation from bone marrow-MSC

Following ethical committee approval (protocol no. 254/15), bone marrow-derived MSCs (bone marrow-MSCs) were isolated from patients at the Policlinico of Modena. Cells were maintained in αMEM (Gibco Wathman, MA, USA) supplemented with 8% platelet lysate plasma (Macopharma, Milano, IT), 1% L-Glutamine (Gibco), 0.2% heparin (Sigma Aldrich, St. Louis, MO, USA), 0.5% ciprofloxacin (Fresenius Kabi). To identify the proper seeding densities, scaffolds were seeded with 2.5×10^4, 5×10^4 and 1×10^5 bone marrow-MSC per scaffold in 15 μL of culture media. To allow cell adhesion, the scaffolds were incubated for 30 min at 37 °C. Then 5 mL of culture media were added and changed every 2–3 days until 4 and 11 days. The detection of cells within 3D structure was performed by 0.04% of crystal violet staining according to previous protocols [39]. Once selected the proper cell density, bone differentiation assay was performed by supplementation of 10 nM β-glicerophosphate (Sigma-Aldrich), 0.1 nM L-Ascorbic acid (Sigma Aldrich), 10 nM dexamethasone (Sigma Aldrich) for 14 days and 100 ng/mL BMP-2 (Peprotech by Thermo Fisher Scientific, Waltham, MA, USA) in the last 7 days. To detect the mineralized matrix, 0.1% Von Kossa and 0.05% Nuclear Fast red staining was performed [39]. Images were acquired using AxioZoom V16 Microscope (Zeiss) equipped with Zen Pro software (Zeiss), objective 1× at magnification of 116 × .

2.9. Immunofluorescence analysis

Immunofluorescence staining was performed on OCs and OBs seeded on biomorphic scaffolds. Mature OCs are multi nucleated cells with ring cytoskeletal rearrangements, detected through positive expression of Tartrate Resistant Acid Phosphatase (TRAP) protein and F-actin Phalloidin staining. OBs were stained with Phalloidin and DAPI as for OCs, and with anti-Osteocalcin antibody to evaluate the expression of osteocalcin, a marker of mature OBs. Briefly, fixed cells were permeabilized with a solution composed by blocking solution (PBS 1× + BSA 1%) with Triton X-100 0.3%, incubated for 5 min at room temperature. Then, in order to evaluate TRAP or osteocalcin expression, cells were incubated for 2 h at room temperature with a primary anti-TRAP antibody (Rabbit, ab185716-Abcam) diluted 1:500 in blocking solution or with a primary anti-osteocalcin antibody (Rabbit, ab198228-Abcam) diluted 1:200 in blocking solution. Cells were washed with PBS 1× and incubated for 1 h with a secondary anti-rabbit conjugated antibody diluted 1:500 in PBS 1× (A-11008, Life Technologies) in dark conditions. For all staining procedures, cells were then washed 3 times with PBS 1× and counterstained with Phalloidin AlexaFluor stock solution (1:40 in PBS 1×) (Life Technologies, Foster City, CA, USA) and DAPI (1:150 in PBS 1×) for 30 min in dark conditions at room temperature. For 2D samples, the cells were then mounted in ProLong gold (Life Technologies) and examined by A1 laser confocal microscopy (Nikon). LIVE/DEAD® Viability/Cytotoxicity Kit (Invitrogen) was performed on MDA-MB-231, MCF-7 and Caki-2 on biomorphic scaffolds at day 1 and day 7 after seeding, according to the manufacturing protocol, and analyzed with A1 laser confocal microscope.

2.10. Culture of ex vivo material from BM patients on biomorphic scaffolds

Patient derived explants (PDEs) were obtained from 2 patients affected by RCC-BM, who underwent surgery, from neoplastic tissue portions selected by an expert pathologist. To obtain PDEs, the tumor tissue was washed once in PBS 1× and manually cut into 5 mm^3 samples. PDEs were cultured in ultra-low attachment 6-well plates, in presence or not of the biomorphic scaffold, in DMEM (Dulbecco's Modified Eagle's Medium, Euroclone) 4.5 g/L glucose, with the addition of 20% non-heat treated FBS, 1% L-glutamine and 1% Penicillin/Streptomycin/amphotericin B (supplements from Life Technologies). PDEs were maintained in culture for up to 7 days at 37 °C and 5% CO_2 in a humidified incubator. The research protocol was approved by both the IRCCS Istituto Romagnolo per lo Studio dei Tumori (IRST) and the Istituto Ortopedico Rizzoli (IOR) Institutional review board and by the Local Ethics Committees (CEROM and AVEC). The Ethical Committee approval number is IRSTB107. The procedures are in accordance with the Helsinki Declaration of 1975, as revised in 2008.

2.11. Viability and necrosis assays of the ex vivo models

Viability and necrosis assays were performed at days 1, 3 and 7 after the starting of the culture. The PDEs viability analyses were performed using the PrestoBlue™ reagent (Invitrogen) following the manufacturer's protocol. In brief, PrestoBlue™ was added at 10% in complete culture medium and incubated for 5 h at 37 °C in the humidified incubator. Subsequently, 100 μL of culture medium were transferred in a 96-well total black plate, absorbance was read and expressed as a ratio between λ 530 and 590 nm (microplate reader Synergy HT, Bio-Tek Instruments Inc.).

The process of cellular necrosis was analyzed through the quantification of the LDH released in culture medium using the LDH-Glo™ Cytotoxicity Assay (Promega), following manufacturer's instructions. Briefly, 4 μL of culture medium of each experimental condition were collected, diluted in 196 μL of LDH storage buffer and stored at −20 °C until testing. Then all samples were diluted in the LDH storage buffer until 1:300 ratio is reached to minimize FBS-derived LDH's interference. After 1 h of incubation, luminescence was recorded through a microplate reader (Synergy HT, Bio-Tek Instruments Inc.).

2.12. Histology

One sample for each experimental condition was sacrificed for histology analyses before starting the culture and on days 3 and 7 after seeding, at the end of the PrestoBlue™ incubation. Specifically, one PDE per condition was collected and divided into two halves: one half was used for IHC, while the other was processed for RNA extraction and gene expression analysis (Section 2.13.2). For histology procedures, PDEs were washed with PBS, fixed in 4% formalin overnight at 4 °C and successively processed for paraffin embedding. Four μm thick histological sections were obtained by formalin-fixed, paraffin-embedded PDEs both from the superficial and from deeper areas of the samples, then stained with hematoxylin & eosin in an automatic slides stainer. Data are shown as viability percentages evaluated by an expert pathologist, considering the percentage of stainable nuclei on the whole tissue section area.

2.12.1. Real time PCR procedure for cell culture experiments

Total RNA from OCs and OBs seeded on biomorphic scaffolds or in 2D condition was isolated using TRIzol Reagent (Invitrogen, Carlsbad, CA, USA) following the manufacturer's instructions. Up to 1 microgram

was reverse-transcribed using the iScript cDNA Synthesis Kit (BioRad, Hercules, CA, USA) or the RevertAid RT Reverse Transcription Kit (Invitrogen, Thermo Fisher Scientific). Real-Time PCR was performed on the 7500 Real-Time PCR System (Applied Biosystems, Foster City, CA, USA) or the QuantStudio 1 Real-Time PCR System (Invitrogen, Thermo Fisher Scientific), using TaqMan gene expression assay mix or SYBR™ Green mix (Applied Biosystems). The stably expressed endogenous *HPRT* or *GAPDH* genes were used as reference and relative gene expression was calculated using the ΔΔCt method [40]. The following markers were analyzed in OCs: Acid Phosphatase 5 - Tartrate Resistant (*ACP5*; the gene encoding TRAP protein), Receptor Activator of Nuclear Factor κ B (*RANK*), Nuclear Factor of Activated T Cells 1 (*NFATC1*), Cathepsin K (*CTSK*). Markers that were analyzed for OBs were the following: Alkaline Phosphatase (*ALPL*), Bone Gamma-Carboxyglutamate Protein - Osteocalcin (*BGLAP*), Collagen Type I Alpha 1 Chain (*COL1A1*) and RUNX Family Transcription Factor 2 (*RUNX2*) (Life Technologies).

2.12.2. Real time PCR procedure for ex vivo experiments

On day 3 and 7 after seeding, one half of each RCC-BM PDEs were freeze-dried in liquid nitrogen and stored at −80 °C upon extraction. Samples were pulverized through mortar and pestle and dissolved in SPK buffer following the instruction of the RNA/DNA/Protein Purification Kit (Norgen Biotek Corp. Thorold, CA) to extract total RNA. The obtained RNA was quantified through Nanodrop ONE (Thermo Fisher, Waltham, MA, USA) and 250 ng were reverse-transcribed using iScript cDNA synthesis kit (Bio-Rad Laboratories, Hercules, CA, USA). The derived cDNA was used to perform gene expression analyses using the Real-time PCR CFX OPUS 96™ detection System (Bio-Rad Laboratories). A SYBR green approach (SsoAdvanced™ Universal SYBR® Green Supermix; Bio-Rad Laboratories) was used to measure relative mRNAs levels of selected apoptosis pathway (*p53, p21, BAX, PUMA*) and osteomimicry target genes (*RANK, RANKL, RUNX 2, ALPL* and *BMP2*).

Differential gene expression was calculated using the 2^DDCt method [40] with respect to the reference gene (*HPRT*). All primers were designed by Qiagen that owns the relative sequences. The respective catalog numbers are listed in Table S1. Only *p21* primers were purchased from Integrated DNA Technologies, Inc. (Coralville, Iowa, USA).

2.13. Cancer-bone cell co-cultures

Co-culture experiments were performed seeding OBs and OCs in the same scaffold, while cancer cells were cultured in a second scaffold functionalized with EVE, meanwhile, anti-RANKL is released by a third scaffold without cells (Fig. 7A). Briefly, at day 0, hMSC were seeded, as previously reported, on a blank scaffold and maintained in complete α-MEM. After 5 days, the differentiation induction of hMSC started with complete α-MEM supplemented with differentiation factors. At day 12, PBMCs isolated from buffycoat, as reported, were seeded on differentiated hMSC and M-CSF was added at the differentiation media. On day 19, blank scaffolds cultured with OBs and OCs derived from PBMCs or THP-1 were placed in indirect co-culture (same well) with EVE-medicated scaffold seeded with Caki-2 or MCF-7 cells, and a medicated scaffold designed to release the anti-RANKL antibody. After 26 days, the co-culture was terminated. The blank scaffold containing OBs and OCs was fixed in 4% paraformaldehyde (PFA) for 15 min. Meanwhile, an MTT assay (Sigma Aldrich, performed according to the manufacturer's protocol) was conducted on the medicated scaffold containing Caki-2 cells.

2.14. Computational modeling of cell behavior and drug treatment

Computational simulations were conducted using SALSA (ScAffoLd SimulAtor), a hybrid continuous discrete cellular automaton that we have previously developed to simulate the behavior of cancer cells cultured in 3D scaffolds [41–43]. Briefly, SALSA combines a discrete and a continuous cellular automaton to describe, respectively, individual cells and the diffusion throughout the culture of relevant molecules (oxygen, glucose and drug). Cancer cells behave according to probabilistic rules that can depend on the local environmental conditions and consume oxygen and glucose at experimentally measured rates [41]. Oxygen, glucose and drug molecules passively diffuse through the virtual structure according to the 2nd Fick's equation. SALSA models for the two BC cell lines (MCF-7, MDA-MB-231) have already been developed and experimentally validated [41,42], while the one describing the Caki-2 population was developed within this work (Fig. S1). No change to the behavioral rules was applied and their parameters were determined as previously described [41,42]. Drug treatment was modeled to reduce proliferation, and a sigmoidal function was used to determine the intensity of the effect [41].

The possibility of treatment release from the medicated scaffold was included. This was implemented by increasing, at each iteration, the drug concentration in each voxel of the virtual scaffold. A quadratic function (Eq. 1), identified to match the drug release measured experimentally, was used to model the increase in drug concentration. It models the amount of drug released by the scaffold (DR) as a function of time (t).

$$DR\ (t) = 0.6075 \cdot ^{2} + 1.613 \cdot t + 5.927 \quad (1)$$

Simulations were conducted for the equivalent of 7 days with treatment being administered at the beginning of the experiment (media supplementation). At least 30 simulations for each condition were conducted. The code and configuration files used for this analysis are available at https://www.mcbeng.it/en/.

2.15. Statistical methods

Each experiment was repeated at least three times and with 3 technical replicates for each condition. Data are presented as mean ± SD. Student's *t*-test or one way analysis of variance (ANOVA) followed by Bonferroni's test were used as appropriate and accepted as significant at $p < 0.05$. For the *ex vivo* PDEs model data were obtained from two different RCC-BM patients. Data were analyzed using GraphPad Prism 8.4.3.3.

3. Results

3.1. Physico-chemical features of drug-loaded biomorphic scaffold

The XRD spectrum of the biomorphic scaffold reports the typical pattern of HA phase with a small amount of β-TCP phase (Fig. 1A) with a ratio of 85/15. The attenuated total reflection (ATR) spectrum confirmed the typical vibrational pattern of HA, particularly all vibration modes of PO_4^{3-}, including the characteristic bands for ν_1, ν_2, ν_3, and ν_4 stretching modes at 963, 472, 1040, and 560–600 cm^{-1} were detected (Fig. 1B).

The total porosity of the examined devices was 53 ± 2%. The microstructure of the biomorphic scaffold revealed a porosity of different dimensions but characterized by two prevalent typologies: a canalicular porosity, which proceeds along the entire length of the material with large sized pores (100–400 μm) and a transversal interconnected porosity of smaller dimensions (1–10 μm) as highlighted in Ruffini et al. [44] (Fig. 1C).

The chemical analysis estimated a Ca/P molar ratio of 1.54 ± 0.02, a Mg (wt%) content of 0.50 ± 0.01 and Sr (wt%) of 0.76 ± 0.01.

3.2. Biomorphic scaffolds sustain the growth and differentiation of bone osteoclasts

A preliminary study of healthy cell growth and behavior was conducted using biomorphic scaffolds without drug functionalization

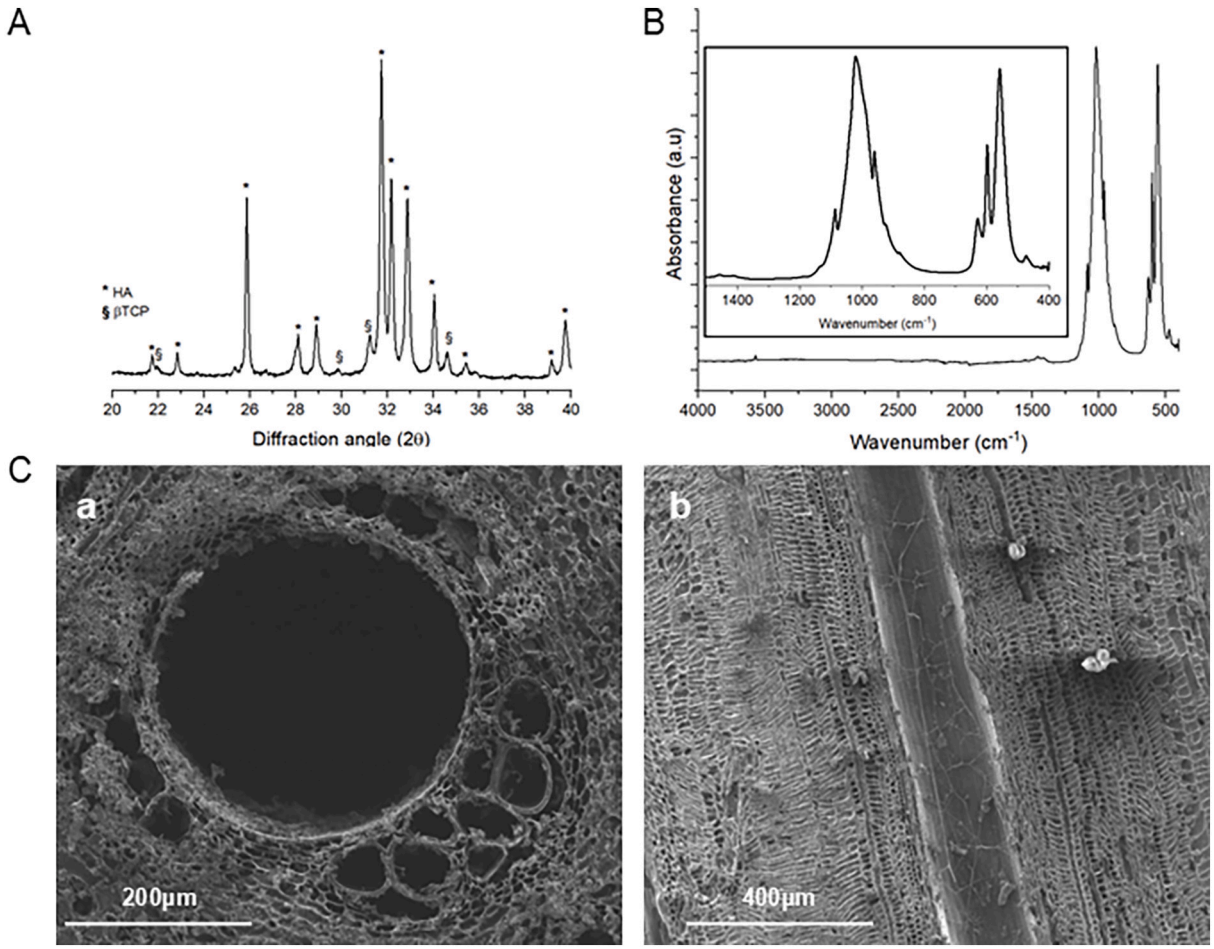

Fig. 1. Synthesis and Characterization of Biomorphic scaffolds. (A) XRD pattern of the biomorphic scaffolds, revealing peaks for both HA and β-TCP; (B) ATR spectrum of biomorphic scaffolds; (C) SEM images of the cross section at 500× of magnification *(a)* and longitudinal section at 250× of magnification *(b)* of the material.

(blank scaffolds) that were populated with the main cellular components of the bone remodeling. The bioactive and bio-conductive properties of biomorphic scaffolds were able to support OCs differentiation from PBMCs. Mature OCs expressing TRAP protein were observed by confocal microscopy after 14 days of differentiation (Fig. 2A), while RT-PCR of *ACP5* gene showed a statistically significant downregulation in the differentiated sample compared to undifferentiated controls (undifferentiated cells) ($p = 0.043$) (Fig. 2B). An increase after 14 days in the gene expression of *RANK* and *CTSK* was observed compared to undifferentiated controls as a proxy of osteoclastogenic differentiation (Fig. 2B). In parallel, data on OCs, derived from the differentiation of THP-1 cells, showed the significantly higher expression of *RANKL* and *ACP5* ($p = 0.001$), the gene encoding for the TRAP protein, confirming the maturation of these progenitors (Fig. 2C).

3.3. Primary MSCs adhered, colonized and differentiated on the biomorphic scaffold

The material efficiently sustained the differentiation of OBs from different precursors. Mature OBs expressing osteocalcin were detected within the scaffolds by confocal microscopy after 14 days of differentiation starting from a commercial primary hMSC (Fig. 3A). Expression of *ALPL,* of the transcription factor *RUNX2* and *COL1A1* were significantly ($p = 0.0000415$; $p = 0.0046$; $p = 0.017$ respectively) higher compared to undifferentiated control, as a measure of osteogenic differentiation (Fig. 3B).

Primary bone marrow-MSC, seeded in the scaffolds at different densities, were able to efficiently colonize the material as visualized in supplementary Fig. 2, after 4 days and 11 from the seeding. Von Kossa staining was performed to assess mineralization and confirm the osteogenic differentiation of primary bone marrow-derived MSCs. As shown in Fig. 3C, a homogeneous dark staining was visible in biomorphic scaffolds with osteogenic medium. Interestingly, dark depots were also observed in the undifferentiated control, suggesting that the biomorphic material itself may possess intrinsic osteoinductive properties. The osteogenic differentiation was further confirmed by real-time PCR data, showing a significant overexpression of *BGLAP* ($p = 0.001$) in differentiated MSCs compared to controls (Fig. 3D). Conversely, no significant upregulation of *RUNX2* was detected, which is consistent with its role as an early osteogenic transcription factor.

3.4. Drug release profiles from loaded scaffolds and preliminary proof of efficacy

The analysis of the release of EVE and anti-RANKL was performed for up to 14 days. A sigmoidal release profile was detected for EVE, with a slow release during the first 5 days (∿10 wt% of loaded drug), followed by a rapid release over the next 48 h (∿40 wt% of loaded drug). From day 7 to day 14 an even slower release was observed (∿50 wt% of loaded drug) (Fig. 4A). Conversely, the anti-RANKL antibody showed an initial rapid release in the first 7 days (Fig. 4B). For the sake of comparison, the released concentration for EVE and of the anti-RANKL antibody after 2 days of immersion were 9.6 µg/mL and 0.09 µg/mL, respectively.

As a proof of the preservation of the drugs' activity, we tested the

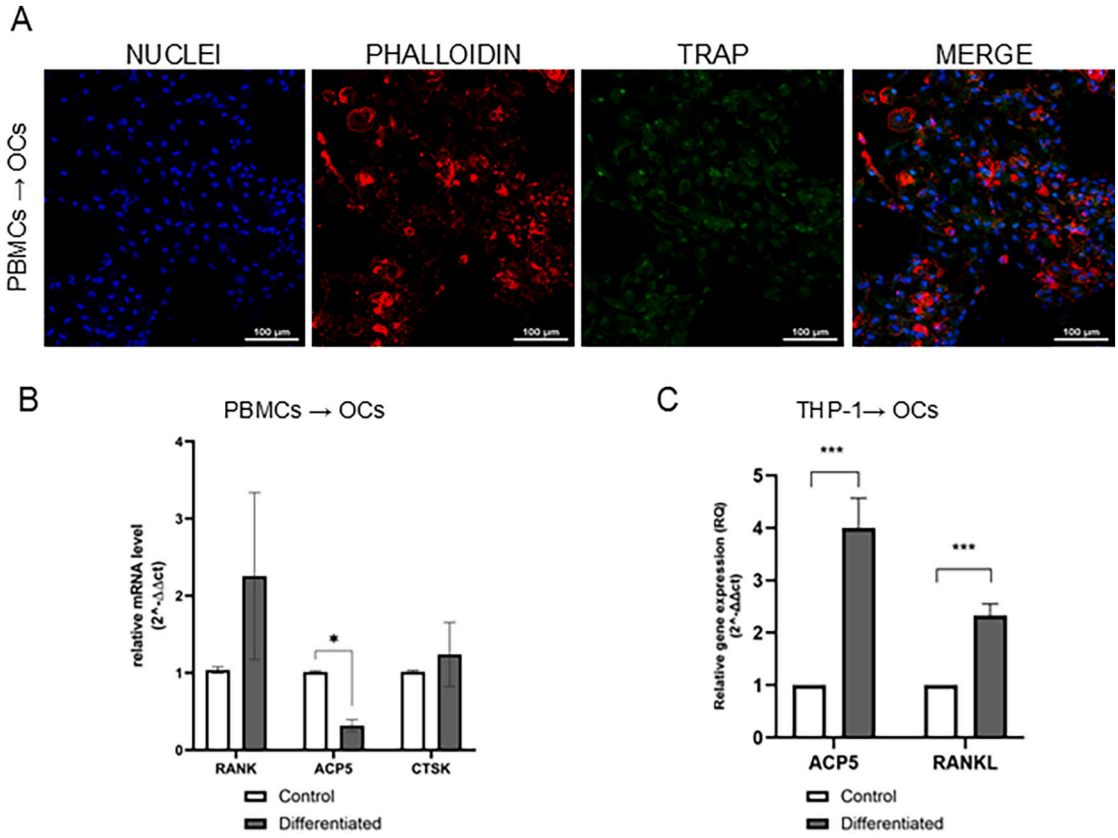

Fig. 2. Differentiation of osteoclasts on biomorphic scaffolds, from THP-1 cell line and PBMCs. (A) Confocal microscopy images of PBMCs in differentiation to osteoclasts at 20× at day 14 of culture. The 3 columns refer to the DAPI staining of nuclei, TRITC staining for Phalloidin, FITC staining to detect TRAP, the staining is merged in the fourth column; B) Gene expression analyses obtained by Real-Time PCR of PBMCs in differentiation to OCs. The reference sample was the negative control of OCs (PBMCs cultured with medium without differentiating growth factors) collected on day 14 of culture. C) Gene expression analyses obtained by Real-Time PCR of THP-1 in differentiation to OCs. The reference sample was the negative control of OCs differentiation collected on day 14 of culture. 2–ΔΔCt method has been used to analyze. Data are mean ± SD. Statistical significance was performed with Student's *t*-test: * $p < 0.05$.

effects of EVE released from biomorphic scaffolds on the two BC cell lines, and we compared results with the direct supplementation of an equal concentration of the drug in the cell culture media (Fig. 5). We tested two different treatment doses and culture conditions. In Fig. 5A was shown the results obtained on MDA-MB-231 and MCF-7 cells cultured in standard 2D monolayer and treated with fresh drug or conditioned media by EVE released from the biomorphic scaffolds. As expected, EVE did not affect the viability of TNBC MDA-MB-231 BC cells at both tested concentrations and methods of administration (Fig. 5A top). On estrogen receptor-positive (ER+) MCF-7 cells, EVE treatment at both doses and administration methods inhibited survival by at least 40%. Interestingly, for the 0.05 µg/mL concentration, EVE efficacy was higher when released from the scaffolds compared to the direct administration (Fig. 5A bottom).

Additionally, we performed a computational analysis using the previously developed SALSA *in silico* framework [41–43], to assess whether the two treatment modalities were associated with differential efficacy according to spatial distribution of cells within the scaffolds (Fig. 5B). When EVE was released from the scaffolds the simulated cell distribution remained approximately uniform for 60–80 h depending on the cell line and drug concentration. On the other hand, media supplementation induced changes early on, with the distribution of MCF-7 and Caki-2 cells showing significant deviations from the initial condition by approximately 20 simulated hours. This effect was less pronounced for the more aggressive MDA-MB-231 BC cell line which is less sensitive to the drug. The more uniform effect of the treatment across the medicated scaffold was maintained throughout the simulation. The final cell distributions were largely uniform for the medicated scaffolds, while the media supplementation condition resulted in a higher cell density in the scaffold's edge where the environmental conditions were more favorable (higher nutrients and oxygen levels, lower drug concentration). The use of a medicated scaffold is also associated with a more effective treatment, with the overall cell density at the end of the simulation being lower than the media supplementation condition. This was confirmed in wet experiments. We evaluated EVE efficacy in MCF-7 cell line cultured directly on the medicated scaffolds, comparing results with fresh EVE supplemented in the culture media of MCF-7 cells cultured on blank scaffolds (Fig. 5C) at both drug concentrations. Comparing the results obtained after 72 h of treatment, the proliferation rate inhibition efficacy of EVE released from the medicated scaffold was higher than the fresh EVE for both the drug concentration (EVE 0.1 µg/mL $p = 0.000035$; EVE 0.05 µg/mL $p = 0.00051$).

3.5. Biomorphic scaffolds efficiently delivered EVE to cancer cells

EVE-medicated scaffolds were used to assess the antitumoral activity of drug-loaded scaffolds, as EVE was expected to exert a growth inhibitory effect on cancer cells. Blank scaffolds were used as control reference. MCF-7, MDA-MB-231 and Caki-2 after 7 days of culturing on blank biomorphic scaffolds preserved their cytoplasm and nucleus morphology when imaged at confocal microscopy. Live/Dead staining showed that blank scaffolds did not affect cell viability after 24 h and 7 days from the seeding (Fig. S2). The proliferation rate of cancer cells grown on blank or medicated scaffolds was assessed from 24 h to 7 days and normalized to the respective 24-h untreated control for comparative analysis. When cells were cultured on EVE-medicated scaffolds, the drug

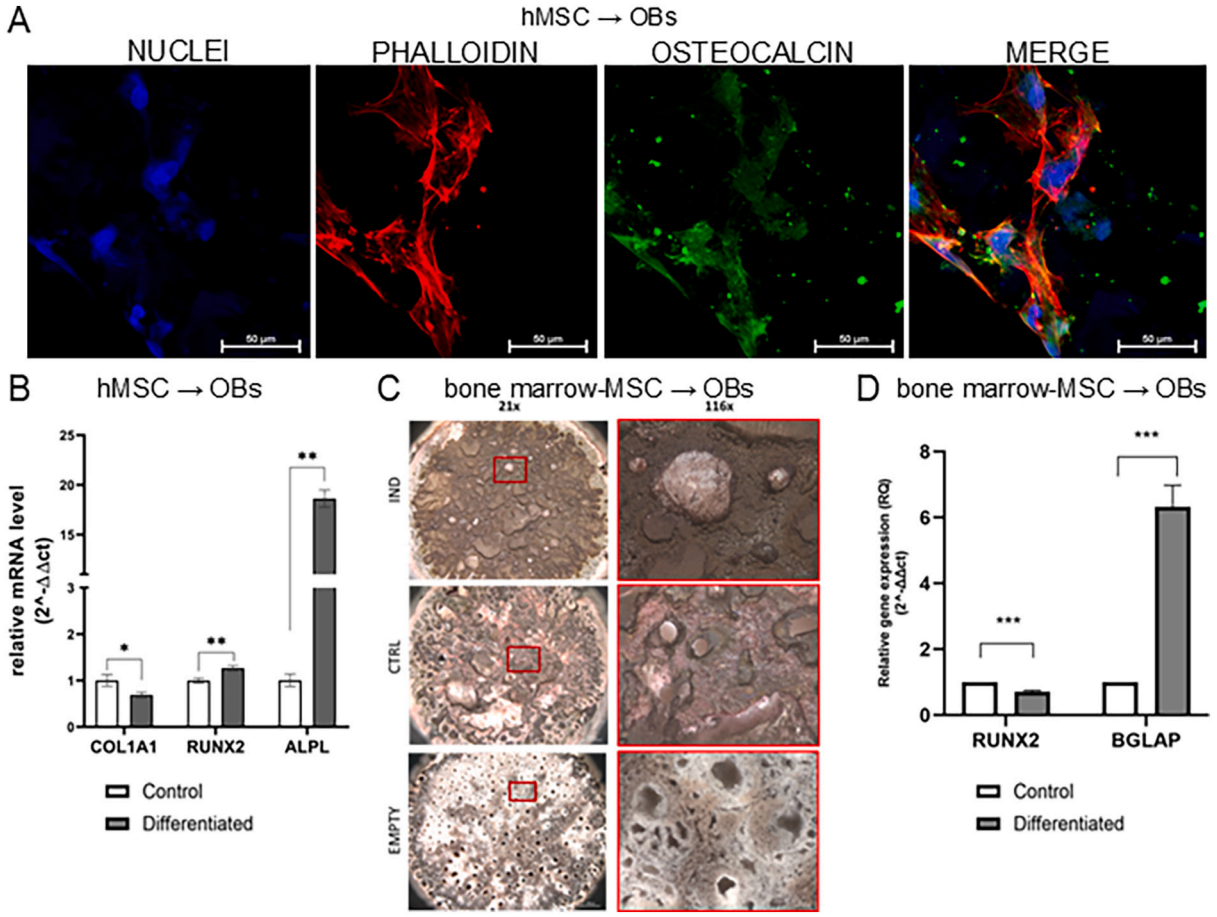

Fig. 3. Differentiation of osteoblasts on biomorphic scaffolds, from hMSC cell line and bone-marrow MSC. (A) Confocal microscopy images of hMSC cell line in differentiation to osteoblasts at 20× at day 14 of culture. The 3 columns refer to the DAPI staining of nuclei, TRITC staining for Phalloidin, FITC staining to detect Osteocalcin, the staining is merged in the fourth column; (B) Gene expression analyses obtained by Real-Time PCR of hMSC in differentiation to OBs. The reference sample was the negative control of OBs (hMSC cultured with medium without differentiating growth factors) collected on day 14 of culture. (C) Von Kossa staining of bone-marrow MSCs seeded on the scaffold and induced to differentiate, compared to non-induced BM-MSCs seeded on the scaffold and the staining of the empty scaffold. (D) Gene expression analyses obtained by Real-Time PCR of bone-marrow MSC in differentiation to OBs. The reference sample was the negative control of OBs differentiation collected on day 14 of culture. 2–ΔΔCt method has been used to analyze. Data are mean ± SD. Statistical significance was performed with Student's t-test: $*p < 0.05$.

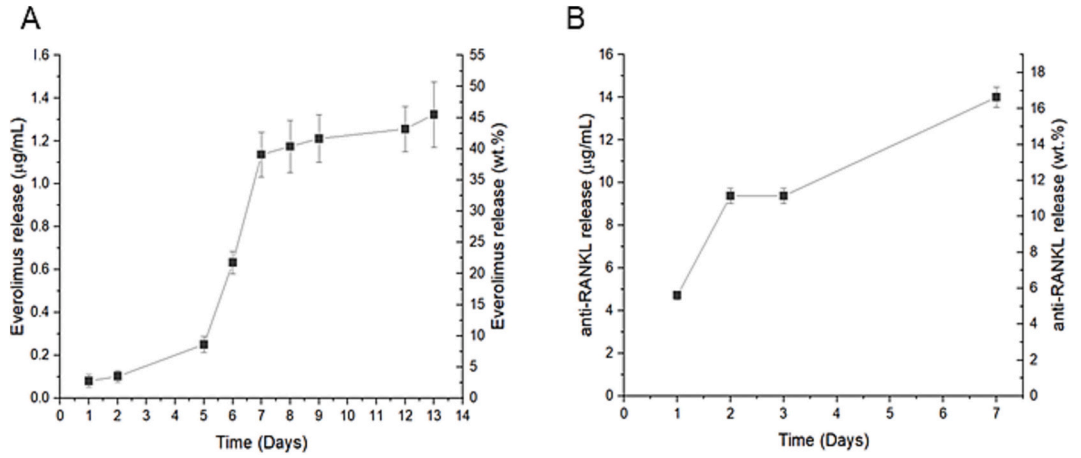

Fig. 4. Drug release profiles from loaded scaffolds. Evaluation of the release profile from biomorphic scaffolds according to UV–visible spectroscopy measurements: (A) Everolimus and (B) anti-RANKL.

released from the material resulted in different levels of growth inhibition according to the intrinsic sensitivity of each cell line. In particular, EVE showed a higher efficacy on ER+ BC MCF-7 and ccRCC Caki-2 cells, with respect to the TNBC MDA-MB-231 BC cells (Fig. 6A). For MCF-7, both drug concentrations significantly impacted cells growth at 72 h (EVE 0.1 μg/mL $p = 0.0000003$; EVE 0.05 μg/mL $p = 2.14E^{-09}$) and at

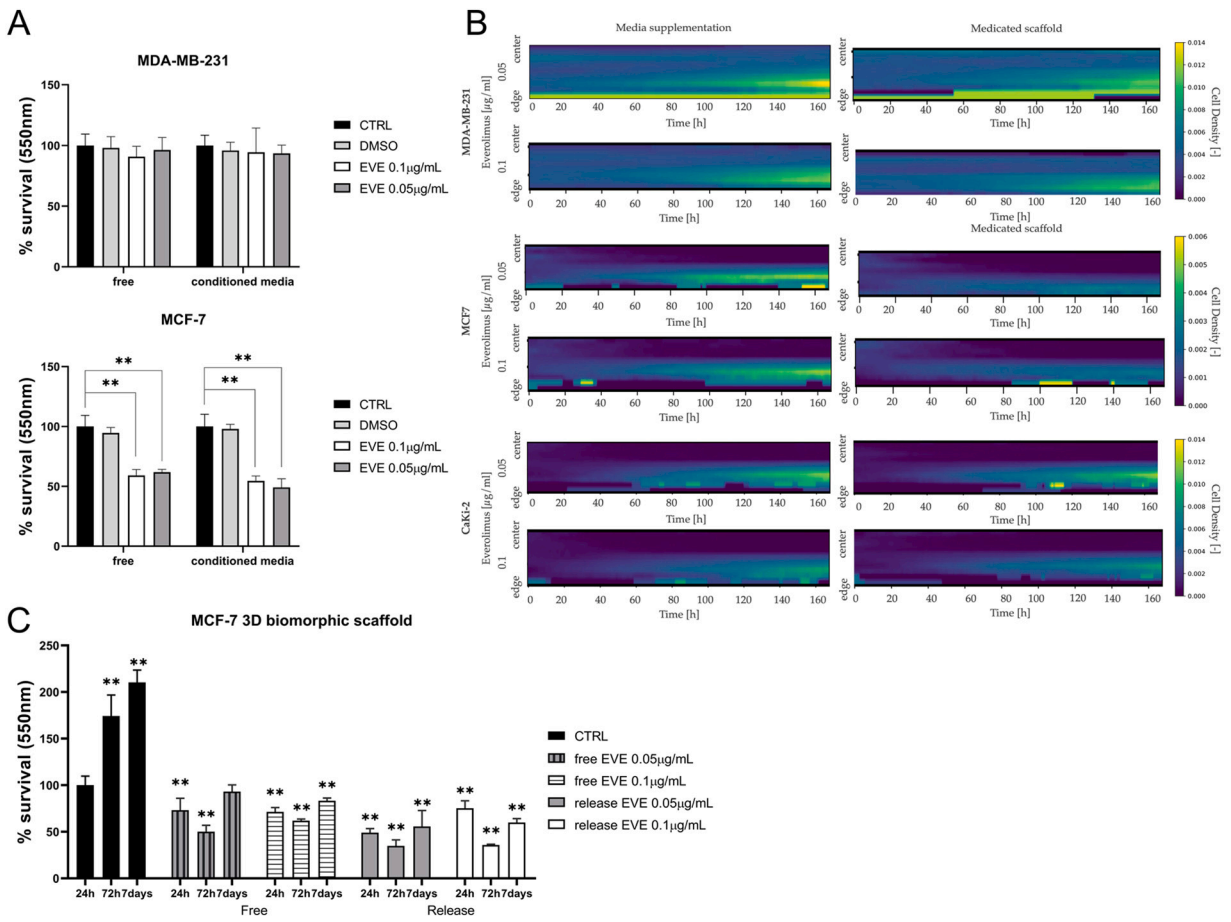

Fig. 5. *In silico* prediction and *in vitro* validation. (A) MDA-MB-231 (top) and MCF-7 (bottom) cell lines viability assays performed on 2D standard cultures to test the impact of EVE released from biomorphic scaffolds (conditioned medium) with respect to fresh EVE added to the medium (free). Data are mean ± SD. $^{**}p < 0.01$; (B) Cell density distribution within the scaffold as simulated by SALSA. Y axis: radial distance from the center of the scaffold, X axis: time (in hours) since the beginning of the simulation. Color shades are the average cell density at each specific time and location (50 simulations for each condition); (C) MCF-7 cell line viability assays performed on 3D biomorphic scaffolds to test the impact of EVE released from biomorphic scaffolds with respect to fresh EVE added to the medium. Data are mean ± SD. $^{**}p < 0.01$. Values were normalized with respect to CTRL not treated at 24 h.

day 7 (EVE 0.1 μg/mL $p = 0.0000015$; EVE 0.05 μg/mL $p = 0.000056$). In particular, the highest concentration of EVE resulted in a growth inhibition of 64% at 72 h and of 40% at day 7, compared to the untreated control (cells growth on the blank scaffold). Treatment with EVE medicated scaffolds also decreased proliferation of Caki-2 at both time points and drug concentration tested (at 72 h EVE 0.1 μg/mL $p = 0.000044$; EVE 0.05 μg/mL $p = 0.0027$; at day 7 EVE 0.1 μg/mL $p = 6.2E^{-12}$; EVE 0.05 μg/mL $p = 8.9E^{-12}$). Concerning MDA-MB-231, a slight effect of the drug was observed only at 72 h, with a growth inhibition of 6% for both concentrations (EVE 0.1 μg/mL $p = 0.03$; EVE 0.05 μg/mL $p = 0.027$). On day 7 cell proliferation was not affected.

3.6. EVE and anti-RANKL released from biomorphic scaffolds impaired OCs survival and differentiation

As both EVE and anti-RANKL were expected to exert an inhibitory activity on osteoclastogenesis, biomorphic scaffolds loaded with 2 different concentrations of EVE, or 1 concentration of anti-RANKL were used to evaluate the effect on PBMCs differentiation into OCs. EVE at both concentrations tested strongly inhibited OCs differentiation as observed by confocal microscopy (Fig. 6B). Few cells were detected on drug-loaded devices after 14 days from the seeding. In addition, no mature OCs were observed, differently from what occurred on blank scaffolds. Conversely, the anti-RANKL antibody did not decrease the cell number, but it blocked PBMCs fusion avoiding the production of mature multinucleated OCs (Fig. 6B).

3.7. EVE and anti-RANKL released from biomorphic scaffolds inhibited cancer cells proliferation in co-culture with bone cells

To further assess the efficacy of medicated biomorphic scaffolds in promoting the inhibition of cancer cell growth while supporting bone regeneration, we seeded a tri-culture of cancer cells, OBs, and OCs in differentiation on medicated scaffolds loaded with the highest drug doses, as single agents or in combination (Fig. 7). The Caki-2 RCC cell line was used for this experiment. Confocal images on Fig. 7B showed that EVE released from the scaffolds was able to impair proliferation of OCs, while the treatment with anti-RANKL resulted in the inhibition of cell differentiation as previously observed for OCs in single culture. Differentiation was almost completely blocked by the scaffolds loaded with both drugs (TRAP staining, Fig. 7B). Conversely, we did not observe a marked decrease in OBs differentiation at all tested conditions (Osteocalcin staining, Fig. 7B). Regarding cancer cells, EVE-medicated scaffolds exerted a growth inhibition of 60% with respect to untreated controls ($p < 2.23E^{-12}$) (Fig. 7C). Anti-RANKL-medicated scaffolds determined an inhibition of cancer cell proliferation of 24% ($p = 0.0015$). Finally, the scaffold medicated with the combination of the two drugs exerted the strongest efficacy, with an inhibition of cancer cell proliferation of 74% ($p = 2.76E^{-11}$) (Fig. 7C).

In parallel, differentiation analysis was conducted using a tri-culture

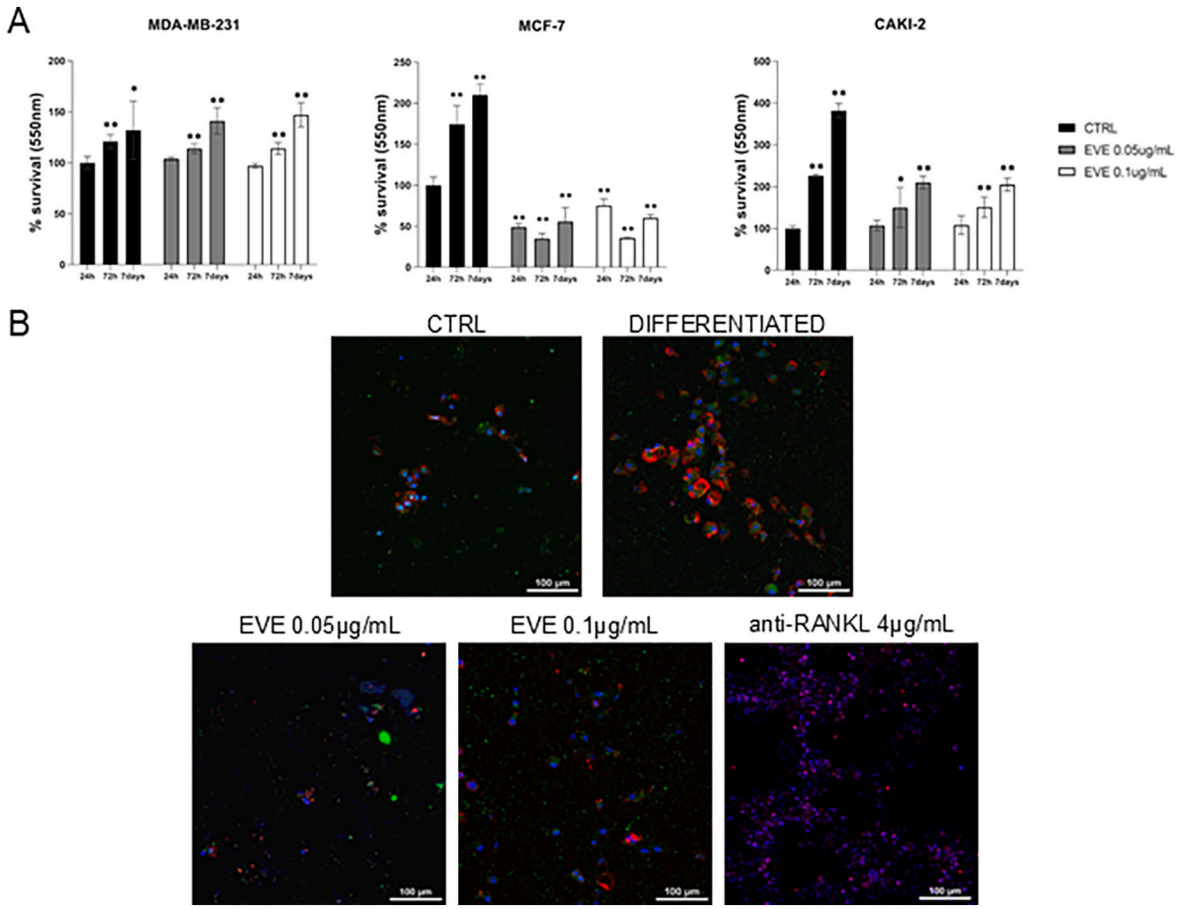

Fig. 6. Impact of mono-medicated biomorphic scaffolds medicated on cancer cells and OCs. (A) MTT assay to evaluate EVE efficacy on cancer cell lines. Absorbance values (550 nm) for each cell line were normalized with respect to the absorbance value of the not treated control samples at 24 h. Data are mean ± SD. $*p < 0.05$, $**p < 0.01$. (B) Confocal images at 20× of OCs differentiated on medicated biomorphic scaffolds. From up to down: CTRL: PBMCs not differentiated, DIFFERENTIATED: PBMCs differentiated in OCs; EVE 0.05 µg/mL: PBMCS in differentiation to OCs in medium added with GFs cultured on biomorphic scaffold medicated with EVE with a release of drug at a concentration of 0.05 µg/mL; EVE 0.1 µg/mL: PBMCS in differentiation to OCs in medium added with GFs cultured on biomorphic scaffold medicated with EVE with a release of drug at a concentration of 0.1 µg/mL; anti-RANKL 4 µg/mL: PBMCS in differentiation to OCs in medium added with GFs cultured on biomorphic scaffold medicated with anti-RANKL with a release of drug at a concentration of 4 µg/mL.

model composed of MCF-7, bone marrow-MSCs and THP-1, cultured on drug-loaded biomorphic scaffolds. The expression of *RUNX2* and *BGLAP*, two key markers of OBs differentiation, was significantly altered by the presence of both drugs. Specifically, a significant downregulation was observed, with relative expression levels of 0.5 for *RUNX2* and 0.4 for *BGLAP* compared to the untreated control condition ($p = 0.001$) (Fig. 7D (a)).

Likewise, the combined treatment impacted on the expression of *ACP5* and *RANKL*, which are genes involved in OCs differentiation. As expected, both were significantly downregulated, with expression values of 0.40 for *ACP5* and 0.25 for *RANKL* ($p = 0.001$) (Fig. 7D(b)).

3.8. Impact of EVE and/or anti-RANKL released from biomorphic scaffolds on RCC-BM patient-derived explants (PDEs)

As a preliminary proof of effectiveness, the viability of the RCC-BM PDEs in presence or absence of blank or drug-loaded biomorphic scaffolds was monitored for up to 7 days and was confirmed over time. For both PDEs samples, the scaffold itself did not significantly influence survival (Fig. 8A), as corroborated by the LDH release quantification as a proxy of cellular necrosis (Fig. 8B). The release of the drug combination showed a modest effect in terms of viability, more evident on Patient 1-PDEs compared to Patient 2-PDEs, and also with respect to single drug administration (Fig. 8A). No biological nor statistically significant differences were noticed regarding the necrosis profiles (Fig. 8B).

To better visualize the impact of the single or combined treatment with EVE and/or anti-RANKL antibody on the whole tissue of the PDE, we performed H&E staining on day 3 and 7 after the seeding. At first glance, representative pictures show that Patient 1-PDEs were intrinsically less viable with respect to Patient 2-PDEs (Fig. 9A). Globally in both cases the presence of the biomorphic scaffold did not alter PDEs tissue architecture or cell viability (Fig. 9A-B.1). Intriguingly, results show no effects of either single or combined drugs administration on Patient 1-PDEs (Fig. 9B.2), while a significant reduction in terms of tissue viability is evident after EVE treatment on day 7 in Patient 2-PDEs (Fig. 9B.2). No differences were observed in case of the combined drug release.

We then proceeded to investigate the effect of the drugs on Patient 2-PDEs at the molecular level (Fig. 9C). We analyzed the expression of some relevant genes involved in the apoptosis pathway and in the osteomimicry phenomenon at day 3 and day 7 after seeding. On day 3, the treatment with EVE led to a *p53* signaling pathways activation, both in the sense of cell cycle arrest (*p21*) and of the apoptosis (*BAX* and *PUMA*). The drug combination caused a less marked activation of the apoptosis pathway in respect to EVE alone (Fig. 9C). On the other hand, a remodulation of osteoblasts markers is visible as a consequence of EVE treatment, both in single and when combined with the anti-RANKL antibody, especially at day 3 (Fig. 9C).

On day 7 instead, the apoptosis pathway is more active in all the experimental conditions (Fig. 9C). Regarding the osteomimicry

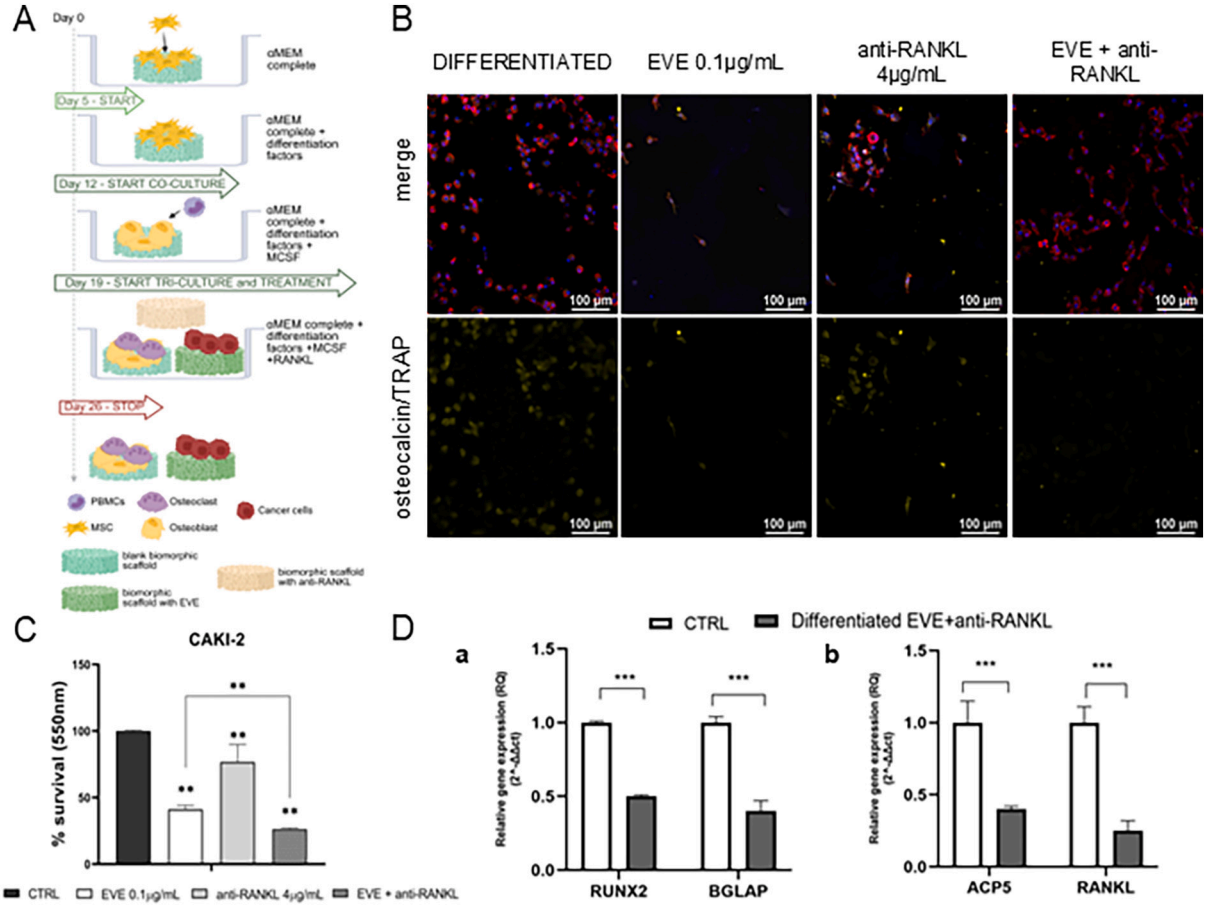

Fig. 7. Co-cultures on biomorphic scaffolds. (A) Scheme of co-culture of bone and cancer cells. Created in https://BioRender.com (B) Confocal microscopy images of hMSC and PBMCS in differentiation to OBs and OCs, respectively, at 20× at day 26 of culture. The first row refers to merged staining of DAPI for nuclei, TRITC for B actin (Phalloidin), the second line refers FITC staining to detect Osteocalcin and TRAP; (C) MTT assay of Caki-2 renal cancer cell line seeded on EVE medicated scaffolds and sharing media with OBs and OCs seeded on a different biomorphic scaffold. Values were normalized with respect to CTRL not treated. Data are mean ± SD. $^{**}p < 0.01$; (D) qPCR quantification of gene expression for osteoblastic differentiation genes *(a)* and osteoclastic differentiation genes *(b)* in scaffolds with cells treated with Everolimus and anti-RANKL, compared to the untreated control (CTRL). 2–ΔΔCt method has been used to analyze. Data are mean ± SD. Statistical significance was performed with Student's t-test: * $p < 0.05$.

phenomenon, the EVE effects particularly on *RUNX2*, *ALPL* and *BMP2* are more pronounced than on day 3 (Fig. 9C). Noteworthy, in both the timepoints, the RCCs that constitute the BM lesion express both *RANK* and *RANKL*.

4. Discussion

Bone metastases significantly affect both patient prognosis and quality of life, making them a critical focus for timely and effective treatment. As a result, there is growing interest in developing innovative therapeutic strategies that can complement and enhance existing treatments throughout the patient's clinical journey. The development of porous materials that mimic natural bone structure and properties has been a key focus in bone tissue regeneration. These scaffolds support cellular activity and interactions, crucial for tissue regeneration while providing structural stability [45,46]. Researchers have explored methods to incorporate drug delivery systems into these scaffolds, such as loading drugs into bioceramics, polymeric matrices, or surface-coated nanoparticles for sustained release [47–49]. Implantable drug delivery systems offer advantages over traditional methods by ensuring localized, controlled drug release, reducing systemic exposure and side effects. In the context of BM, the chance to enrich the bone scaffold with specific antiresorptive and/or antineoplastic drugs has the potential to be a concrete improvement for the bioimplant success. The most common method for optimizing grafts in the treatment of osteolysis is by functionalizing them with anti-osteolytic drugs. For instance, bone cements loaded with zoledronic acid have been shown to inhibit malignant or metastatic bone tumors while simultaneously acting as a bone scaffold [50,51]. In a study by Ewa Oledzka et al., a new multifunctional composite was developed as a promising bone scaffold, consisting of HA porous granules doped with selenite ions (SeO_3^{2-}) and conjugated to a biodegradable branched copolymer-bisphosphonate. This composite was designed to deliver pamidronate locally, effectively inhibiting bone resorption and OCs activity [52]. Other approaches include the development of a local drug delivery system using calcium phosphate cement (CPC) as a carrier for chemotherapeutics. CPC loaded with paclitaxel was tested on osteosarcoma and metastatic BC cells [53]. The study found that CPC effectively retains and releases chemotherapeutics, making it a promising vector for localized drug delivery in BM treatment [53]. Other strategies involve additive manufacturing (3D printing) to create customized implants with improved reproducibility and cost-effectiveness. Angahar et al. developed a 3D printed medicated porous scaffold for the local delivery of doxorubicin (DOXO) in BM. These scaffolds released 60–75% of DOXO over seven days, significantly reducing cancer cell activity and proliferation. This method could locally deliver drugs at tumor sites, reduce systemic side effects, enhance bone healing, and improve patient outcomes [54]. However, it has been observed that such a type of polymeric scaffolds undergoes non-metabolic dissolution inducing aberrant cell behavior [55].

The aim of this work is to develop an innovative multiple action

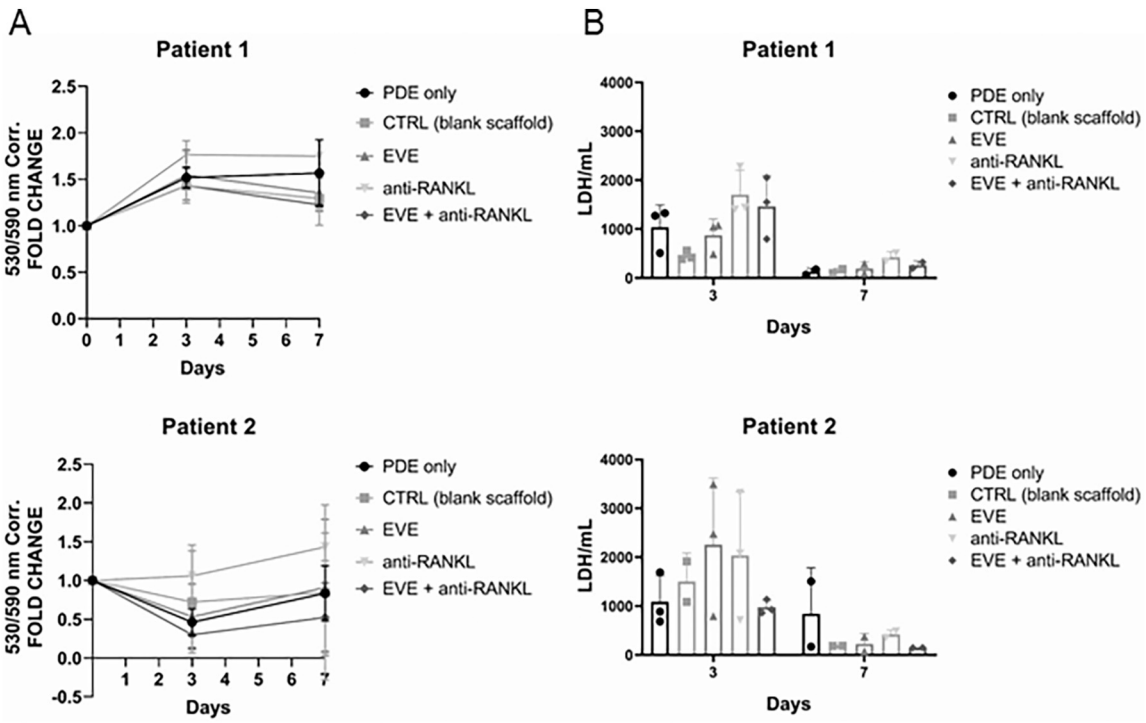

Fig. 8. Effects of black or medicated biomorphic scaffolds on PDEs viability. Top Patient 1; bottom Patient 2. (A) Viability assay performed on PDEs using Presto Blue® reagent at day 1, 3 and 7 after seeding. (B) Quantification of released LDH in the medium at days 1, 3 and 7 as a proxy of cellular necrosis. For each experiment three PDEs per condition were used. Both assays have been performed on the same PDEs.

device that combines targeted anticancer therapy with enhanced bone regeneration. This is achieved through the integration of anti-osteolytic and antitumoral drugs into a biomorphic bone scaffold, characterized by its strong regenerative capabilities. The rattan-derived bone scaffold was discovered in 2009 by Tampieri et al. [56] Since then, it has been subject to chemical and physical characterization, as well as testing in animal models [31] and in different clinical indications [57–59]. Each of these studies have demonstrated unique mechanical and osteoinductive properties [31–34], making it ideal for bone tissue regeneration. In addition, its hierarchically organized porosity [44] is suitable for drug encapsulation and release [36] as necessary in this particular study. Firstly, we confirmed the biocompatibility of biomorphic scaffolds on healthy bone cells showing that MSCs and PBMCs/THP-1 seeded on blank scaffolds successfully differentiated into mature cells OBs and OCs, respectively. Similar results were obtained starting from two different sources of primary MSCs. These findings confirm that this material can support the physiological growth of healthy bone tissue. Next, the scaffolds were functionalized with two drugs, EVE and an anti-RANKL antibody. These drugs not only contribute to inhibiting bone resorption but may help restore the bone tissue homeostasis. EVE disrupts the early phase of OCs maturation, while the anti-RANKL antibody inhibits the late phase of this process [8,9]. Moreover, EVE itself provides an antitumoral effect and it is used in clinical practice for the treatment of metastatic hormone receptor-positive BC [60] and RCC [61]. In this work, we developed an easy-to-use protocol for drug functionalization designed for ease of use by non-expert personnel, including operating room staff. The method ensures a controlled drug release profile without compromising the drug's efficacy on target cells (as demonstrated in Fig. 5). We challenged EVE medicated scaffolds on 3 selected cancer cell lines. Released EVE at both tested concentrations showed a higher effect on ER+ MCF-7 and Caki-2 cells corresponding to the breast and renal cancer histotypes for which EVE is clinically indicated, compared to its effect on TNBC cells. In fact, TNBC is usually subjected to a different therapeutic schedule. Regarding bone cells and specifically OCs, EVE and anti-RANKL medicated scaffolds were able to impair OCs maturation. This result confirms the assumption that the medicated scaffold can help bone homeostasis restoration on a resected lytic BM characterized by a high rate of resorption.

A key aspect refers to the sterilization procedures that may significantly affect the stability and bioactivity of loaded therapeutics, especially protein-based agents such as anti-RANKL antibodies. While Everolimus, as a small hydrophobic molecule, is expected to maintain relatively favorable stability in dry conditions, the long-term preservation of antibody functionality following adsorption onto apatite surfaces remains to be systematically evaluated, as protein adsorption may induce conformational changes or aggregation phenomena affecting the antigen-binding activity. Importantly, although these aspects were beyond the scope of the present study, the biological activity of the released therapeutics was successfully confirmed through the performed *in vitro* assays, supporting the feasibility of the loading and release strategy adopted in this work and providing a preliminary indication that the functionalization procedure did not impair the therapeutic efficacy of the delivered agents. Future studies should therefore assess shelf-life, storage conditions, and residual biological activity after sterilization and prolonged storage. The biomorphic apatite scaffolds exhibited favorable handling characteristics and adaptability during manipulation; however, further optimization of mechanical reliability in clinically relevant load-bearing conditions will be important for future translational development. From a translational perspective, a clinically advantageous strategy could involve sterilization of the biomorphic scaffold prior to functionalization, followed by intraoperative drug loading under sterile conditions. Such an approach may minimize potential alterations in therapeutic bioactivity associated with terminal sterilization procedures and simultaneously reduce challenges related to the long-term shelf-life and storage stability of pre-functionalized scaffolds.

It has long been known that preclinical testing should include the contribution of the tumor microenvironment (TME) that can alter the characteristics of cancer cells including their drug susceptibility. Here we modeled the tumor-TME interaction using indirect co-culturing of

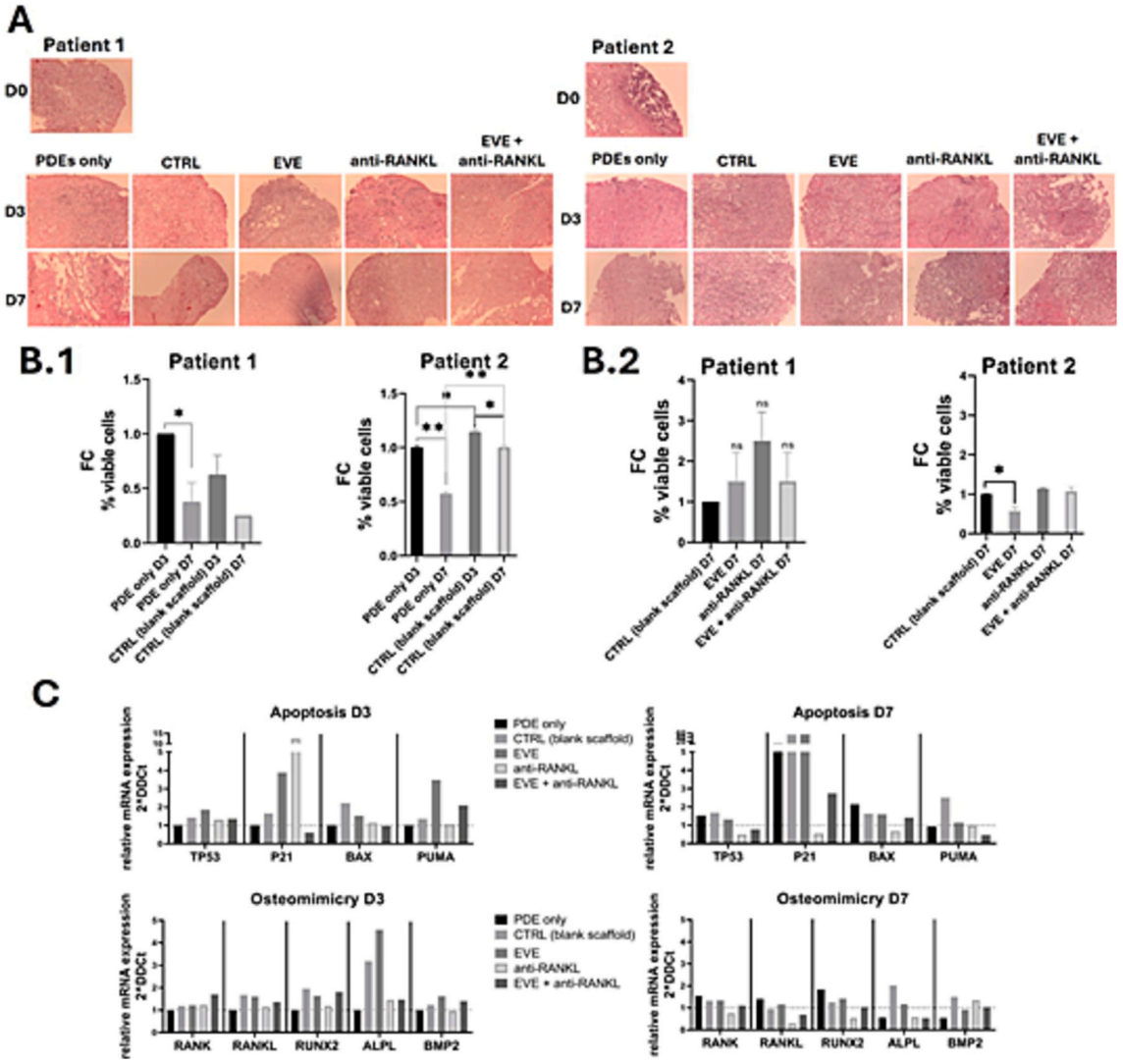

Fig. 9. Impact of blank or medicated biomorphic scaffolds on PDEs tissue viability and molecular profile. (A) Representative pictures of H&E staining of patients' original BM-tissue (Day 0) and of PDEs-FFPE slides at day 3 and 7 after seeding. The images are taken from the inner part of the PDE and performed at 10× magnification. B) Percentage of viable cells evaluated on the whole tissue area considering stainable/viable nuclei. Results are shown as fold change with respect to PDEs only D3 (B.1) and on CTRL (blank scaffold) D7 (B.2). (C) Gene expression analyses on days 3 and 7 of genes involved in the apoptosis (upper panel) and osteomimicry (bottom panel) pathways. Data are shown as descriptive trends resulting from the arithmetic mean of a technical triplicate due to limited sample size. The PDEs are the same used for viability and necrosis experiments shown in Fig. 8. On day 3 and 7 one PDEs per condition was sacrificed and cut into halves, of which each one was used for IHC and one for RNA extraction and gene expression procedures.

OCs, OBs and cancer cells, as well as *ex vivo* PDEs. For the co-culture experiments ER+ MCF-7 and RCC Caki-2 were used as these two tumor subtypes have indications for treatment with EVE in the clinical setting. Co-culture experiments of bone with cancer cells demonstrated an additive effect on OCs inhibition in the presence of both drugs compared to single agents. Although anti-RANKL is primarily known for its effects on OCs inhibition, it also led to a 25% reduction in the growth of renal Caki-2 cancer cells in this co-culture setting. The combination of both drugs demonstrated the strongest efficacy, inhibiting cancer cell proliferation by up to 70%. In line with this, differentiation analysis conducted within the triculture setting, comprising bone marrow-MSCs, THP-1, and MCF-7 cells, revealed a significant downregulation of key osteoblastic and osteoclastic markers, including *RUNX2*, *BGLAP*, *ACP5*, and *RANKL*, in the presence of both drugs, suggesting that the combination of EVE and anti-RANKL may interfere with bone cell maturation through indirect, microenvironment-mediated mechanisms (Fig. 7D). These findings overall demonstrate that biomorphic scaffolds functionalized with EVE and anti-RANKL can effectively modulate the differentiation of osteoblast and osteoclast, supporting their potential role in regulating the crosstalk between cancer cells and the bone niche.

To increase the translational relevance of our results, we challenged the medicated scaffolds with RCC-PDEs. PDEs represent a reliable and upgraded research tool with respect to standard cell cultures mainly due to the maintenance of a 3D tissue architecture and TME components that allow the obtainment of robust results in different solid tumors and also in co-clinical trials [62,63]. In this work, we cultivated PDEs through the free floating method, finding that tissue viability decreases over 7 days in static culture (Fig. 8). Nevertheless, drug efficacy was still measurable and comparable through the use of different technical approaches, namely metabolic assays, IHC staining and gene expression analyses (Figs. 8–9). Additionally, this model allowed us to detect drug effects not only on the cancer cells but also on the TME. Indeed, the observed increased expression of OBs markers such as *RUNX2*, *ALPL*, and *BMP2* - particularly in the initial phase of *ex vivo* culture - may be linked to EVE's effects. Moreover, the biomorphic scaffold itself contributed to bone regeneration, with a more pronounced effect when both drugs were

present. By day 7, the inhibitory effect of the anti-RANKL antibody became more evident. Altogether, our data suggest that treatment with EVE and/or anti-RANKL may be beneficial for a subset of RCC-BM patients and that this effect can be evaluated using the PDEs model. Interestingly, to further endorse the use of PDEs model in preclinical settings, in Patient 2-PDEs, we observed that RCC-BM cells expressed both *RANK* and *RANKL*, indicating their osteomimicry ability. This phenomenon, previously reported in BC-BM by Pantano et al. [64], may be a relevant feature also in RCC-BM. Altogether, these findings support the potential of PDEs as a good preclinical model to evaluate drug efficacy and test novel biomaterials for BM treatment. We emphasize the importance of combining complementary assays to evaluate similar outcomes in order to strengthen the robustness and reliability of the results.

Undoubtedly, in addition to increasing the number of patients included in the preclinical validation, our PDE model needs further refinement. For instance, future development may include the incorporation of a dynamic environment using millifluidic devices and eventually the exploitation for the development of a platform for screening standard or innovative treatments offering the added advantage of applying the 3R principle before proceeding with *in vivo* studies.

To integrate and support the wet lab experiments, we took advantage of the SALSA software, an *in silico* tool we previously developed [41–43], to simulate cell distribution and drug effect of medicated scaffolds. SALSA provided access to information that is difficult to obtain through wet experiments. Interestingly, it revealed that cells tend to migrate from the center to the edge of the scaffold, where environmental conditions - such as higher nutrient and oxygen levels and lower drug concentrations - are more favorable. This effect was most pronounced at the lowest EVE concentration. Moreover, SALSA successfully predicted differences in cancer cell responses to EVE, depending on whether the drug was released from medicated scaffolds or supplemented directly into the culture medium. *In silico* results revealed that the lowest EVE concentration delivered *via* the medicated scaffold produced effects remarkably similar to those observed with the highest drug concentration in the media supplementation condition. Experimental data confirmed SALSA's predictions, demonstrating the strong performance of our in-house developed software. This tool will be instrumental in guiding future experimental research, reducing the need for wet experiments, and enhancing the overall drug validation process.

Taken together, results on co-cultures, PDEs and *in silico* models support our original hypothesis, namely the chance to develop regenerative functionalized materials that efficiently combine anti-tumor therapy (EVE) with a bone regeneration (anti-RANKL antibody) drug.

5. Conclusion

Medicated bone scaffolds offer a transformative approach to treat BM by providing localized, sustained drug delivery, enhanced therapeutic efficacy while minimizing systemic side effects. In this work, we developed biomorphic scaffolds endowed with multiple actions, including effective drug release providing inhibition of tumor growth and anti-resorptive character, associated also to new bone regeneration stimuli, thus addressing both oncological and orthopedic challenges. This innovative strategy may be applied in metastatic patients eligible for surgery, based on the hypothesis that combining a biomimetic bone regenerative material with the two selected drugs could accelerate recovery of damaged tissue at lytic BM site, potentially revolutionizing clinical practice. Further validations, including *in vivo* testing, are warranted to confirm this hypothesis.

CRediT authorship contribution statement

Claudia Cocchi: Writing – original draft, Visualization, Validation, Methodology, Investigation, Formal analysis, Conceptualization. **Valentina Bergamini:** Writing – original draft, Methodology, Investigation, Formal analysis. **Monica Montesi:** Writing – review & editing, Validation, Supervision, Methodology, Data curation. **Laura Mercatali:** Writing – original draft, Supervision, Project administration, Funding acquisition, Formal analysis, Conceptualization. **Massimiliano Dapporto:** Writing – review & editing, Writing – original draft, Visualization, Validation, Methodology, Investigation, Formal analysis. **Marta Tavoni:** Writing – review & editing, Writing – original draft, Visualization, Validation, Methodology, Investigation, Formal analysis. **Chiara Spadazzi:** Writing – review & editing, Formal analysis, Conceptualization. **Alessandro De Vita:** Writing – review & editing, Conceptualization. **Giacomo Miserocchi:** Writing – review & editing, Conceptualization. **Silvia Vanni:** Writing – review & editing, Conceptualization. **Giulia Sbanchi:** Writing – review & editing, Methodology. **Marilisa Cortesi:** Writing – original draft, Software. **Emanuele Giordano:** Writing – review & editing, Software, Funding acquisition. **Roberto Casadei:** Writing – review & editing. **Giacomo Morozzi:** Writing – review & editing. **Alberto Ballardini:** Writing – original draft. **Ania Naila Guerrieri:** Writing – original draft, Methodology, Formal analysis. **Enrico Lucarelli:** Writing – original draft, Funding acquisition, Conceptualization. **Chiara Bellotti:** Writing – review & editing, Methodology, Formal analysis. **Marco Gambarotti:** Writing – review & editing. **Davide Maria Donati:** Writing – review & editing. **Elena Veronesi:** Writing – review & editing, Methodology, Funding acquisition. **Massimo Dominici:** Supervision, Funding acquisition, Conceptualization. **Simone Sprio:** Writing – review & editing, Funding acquisition, Conceptualization. **Anna Tampieri:** Writing – review & editing, Funding acquisition, Conceptualization. **Alberto Bongiovanni:** Writing – review & editing, Project administration, Funding acquisition, Conceptualization. **Chiara Liverani:** Writing – review & editing, Project administration, Funding acquisition, Formal analysis, Conceptualization. **Toni Ibrahim:** Writing – review & editing, Supervision, Project administration, Funding acquisition, Conceptualization.

Ethic statement

The research protocol was approved by both the IRCCS Istituto Romagnolo per lo Studio dei Tumori (IRST) and the Istituto Ortopedico Rizzoli (IOR) Institutional review board and by the Local Ethics Committees (CEROM and AVEC). The Ethical Committee approval number is IRSTB107. The procedures are in accordance with the Helsinki Declaration of 1975, as revised in 2008. Peripheral blood mononuclear cells (PBMCs) were isolated from buffy coats of healthy donors who gave written informed consent to take part in the study.

Declaration of Generative AI and AI-assisted technologies in the writing process

In this work generative artificial intelligence (AI) has not been used.

Funding

This research project was funded by Regione Emilia Romagna, POR-FESR 2014–2020, Project n. PG/2018/632022. The work was partly supported thanks to the contribution of Ricerca Corrente by the Italian Ministry of Health.

Declaration of competing interest

The authors declare no competing interest.

Acknowledgements

The authors would like to thank Regione Emilia Romagna to have funded this research project. Authors are grateful to the MUSCULOSKELETAL TUMOR BIOBANK (BIOTUM) - member of the CRB-IOR - which provided us the biological samples.

Appendix A. Supplementary data

Supplementary data to this article can be found online at https://doi.org/10.1016/j.bioadv.2026.215029.

Data availability

Data will be made available on request.

References

[1] H. Kennecke, R. Yerushalmi, R. Woods, M.C. Cheang, D. Voduc, C.H. Speers, T. O. Nielsen, K. Gelmon, Metastatic behavior of breast cancer subtypes, J. Clin. Oncol. 28 (2010) 3271–3277, https://doi.org/10.1200/JCO.2009.25.9820.

[2] R.E. Coleman, P.I. Croucher, A.R. Padhani, P. Clézardin, E. Chow, M. Fallon, T. Guise, S. Colangeli, R. Capanna, L. Costa, Bone metastases, Nat. Rev. Dis. Primers 6 (2020) 83, https://doi.org/10.1038/s41572-020-00216-3.

[3] N. Sethi, Y. Kang, Unravelling the complexity of metastasis - molecular understanding and targeted therapies, Nat. Rev. Cancer 11 (2011) 735–748, https://doi.org/10.1038/nrc3125.

[4] R.E. Coleman, Clinical features of metastatic bone disease and risk of skeletal morbidity, Clin. Cancer Res. 12 (2006) 6243–6249, https://doi.org/10.1158/1078-0432.CCR-06-0931.

[5] M. Santoni, A. Conti, G. Procopio, C. Porta, T. Ibrahim, S. Barni, F.M. Guida, A. Fontana, A. Berruti, R. Berardi, et al., Bone metastases in patients with metastatic renal cell carcinoma: are they always associated with poor prognosis? J. Exp. Clin. Cancer Res. 34 (2015) 10 https://doi.org/10.1186/s13046-015-0122-0.

[6] D. Santini, G. Procopio, C. Porta, T. Ibrahim, S. Barni, C. Mazzara, A. Fontana, A. Berruti, R. Berardi, B. Vincenzi, et al., Natural history of malignant bone disease in renal cancer: final results of an Italian bone metastasis survey, PLoS One 8 (2013) e83026, https://doi.org/10.1371/journal.pone.0083026.

[7] J.B. Easton, P.J. Houghton, mTOR and cancer therapy, Oncogene 25 (2006) 6436–6446, https://doi.org/10.1038/sj.onc.1209886.

[8] F. Bertoldo, F. Silvestris, T. Ibrahim, F. Cognetti, D. Generali, C. Ripamonti, I., D. Amadori, M.A. Colleoni, P. Conte, L. Del Mastro, et al., Targeting bone metastatic cancer: role of the mTOR pathway, Biochim. Biophys. Acta 1845 (2014) 248–254, https://doi.org/10.1016/j.bbcan.2014.01.009.

[9] L. Mercatali, C. Spadazzi, G. Miserocchi, C. Liverani, A. de Vita, A. Bongiovanni, F. Recine, D. Amadori, T. Ibrahim, The effect of everolimus in an in vitro model of triple negative breast cancer and osteoclasts, Int. J. Mol. Sci. 17 (2016), https://doi.org/10.3390/ijms17111827.

[10] M. Esposito, T. Guise, Y. Kang, The biology of bone metastasis, Cold Spring Harb. Perspect. Med. 8 (2018) a031252, https://doi.org/10.1101/cshperspect.a031252.

[11] M. Esposito, Y. Kang, Targeting tumor-stromal interactions in bone metastasis, Pharmacol. Ther. 141 (2) (2014 Feb) 222–233, https://doi.org/10.1016/j.pharmthera.2013.10.006 (Epub 2013 Oct 15).

[12] K. Fizazi, M. Carducci, M. Smith, R. Damião, J. Brown, L. Karsh, P. Milecki, N. Shore, M. Rader, H. Wang, et al., Denosumab versus zoledronic acid for treatment of bone metastases in men with castration-resistant prostate cancer: a randomised, double-blind study, Lancet 377 (2011) 813–822, https://doi.org/10.1016/S0140-6736(10)62344-6.

[13] A.T. Stopeck, A. Lipton, J.J. Body, G.G. Steger, K. Tonkin, R.H. de Boer, M. Lichinitser, Y. Fujiwara, D.A. Yardley, M. Viniegra, et al., Denosumab compared with zoledronic acid for the treatment of bone metastases in patients with advanced breast cancer: a randomized, double-blind study, J. Clin. Oncol. 28 (2010) 5132–5139, https://doi.org/10.1200/JCO.2010.29.7101.

[14] L. Moretti, L. Richelmi, D. Cosentini, R. Pedersini, S. Grisanti, V. Amoroso, A. Berruti, M. Laganà, Adjuvant denosumab for early breast cancer-Evidence and controversy, Breast 78 (2024) 103826, https://doi.org/10.1016/j.breast.2024.103826.

[15] C. Errani, A. Bazzocchi, P. Spinnato, G. Facchini, L. Campanacci, G. Rossi, A. F. Mavrogenis, What's new in management of bone metastases? Eur. J. Orthop. Surg. Traumatol. 29 (2019) 1367–1375, https://doi.org/10.1007/s00590-019-02446-y.

[16] C. Errani, A.F. Mavrogenis, L. Cevolani, S. Spinelli, A. Piccioli, G. Maccauro, N. Baldini, D. Donati, Treatment for long bone metastases based on a systematic literature review, Eur. J. Orthop. Surg. Traumatol. 27 (2017) 205–211, https://doi.org/10.1007/s00590-016-1857-9.

[17] E. Ortiz-Cruz, M.C. Gebhardt, L.C. Jennings, D.S. Springfield, H.J. Mankin, The results of transplantation of intercalary allografts after resection of tumors. A long-term follow-up study, J. Bone Joint Surg. Am. 79 (1997) 97–106, https://doi.org/10.2106/00004623-199701000-00010.

[18] Y. Tsuda, H. Yasunaga, H. Horiguchi, K. Fushimi, H. Kawano, S. Tanaka, Complications and postoperative mortality rate after surgery for pathological femur fracture related to bone metastasis: Analysis of a nationwide database, Ann. Surg. Oncol. 23 (2016) 801–810, https://doi.org/10.1245/s10434-015-4881-9.

[19] J. Li, L. Qin, K. Yang, Z. Ma, Y. Wang, L. Cheng, D. Zhao, Materials evolution of bone plates for internal fixation of bone fractures: A review, J. Mater. Sci. Technol. 36 (2020) 190–208, https://doi.org/10.1016/j.jmst.2019.07.024.

[20] S. Sequeira, M.H. Fernandes, N. Neves, M.M. Almeida, Development and characterization of zirconia-alumina composites for orthopedic implants, Ceram. Int. 43 (2017) 693–703, https://doi.org/10.1016/j.ceramint.2016.09.216.

[21] T. Liu, Q. Zhang, X. Guo, X. Zhang, Z. Li, X. Li, Treatment and outcome of malignant bone tumors of the proximal humerus: biological versus endoprosthetic reconstruction, BMC Musculoskelet. Disord. (2014) 69, https://doi.org/10.1186/1471-2474-15-69, 15.

[22] J.M. Bouler, P. Pilet, O. Gauthier, E. Verron, Biphasic calcium phosphate ceramics for bone reconstruction: A review of biological response, Acta Biomater. 53 (2017) 1–12, https://doi.org/10.1016/j.actbio.2017.01.076.

[23] M. Trzaskowska, V. Vivcharenko, A. Przekora, The impact of hydroxyapatite sintering temperature on its microstructural, mechanical, and biological properties, Int. J. Mol. Sci. 24 (2023) 5083, https://doi.org/10.3390/ijms24065083.

[24] W. Wang, K.W.K. Yeung, Bone grafts and biomaterials substitutes for bone defect repair: A review, Bioact. Mater. 2 (2017) 224–247, https://doi.org/10.1016/j.bioactmat.2017.05.007.

[25] P. Ahangar, M. Aziz, D.H. Rosenzweig, M.H. Weber, Advances in personalized treatment of metastatic spine disease, Ann. Transl. Med. 7 (2019) 223, https://doi.org/10.21037/atm.2019.04.41.

[26] P. Hernigou, J.P. Thiéry, J. Benoit, M.C. Voisin, P. Leroux, G. Hagege, G. Delepine, D. Goutallier, Methotrexate diffusion from acrylic cement. Local chemotherapy for bone tumours, J. Bone Joint Surg. (Br.) 71 (1989) 804–811, https://doi.org/10.1302/0301-620X.71B5.2584251.

[27] I. Pountos, P.V. Giannoudis, Drug-eluting implants for the suppression of metastatic bone disease: current insights, Expert Rev. Med. Devices 15 (4) (2018) 301–311, https://doi.org/10.1080/17434440.2018.1456336.

[28] Y. Zhao, W. Wang, M. Liu, et al., Mn_3O_4-potentiated bifunctional hydrogel for mild temperature-controlled tumor ablation and osteogenesis, Bioact. Mater. 55 (2025) 391–409. Published 2025 Sep 25, https://doi.org/10.1016/j.bioactmat.2025.09.037.

[29] R. Liu, Q. Liang, J.Q. Luo, et al., Ferritin-based nanocomposite hydrogel promotes tumor penetration and enhances cancer chemoimmunotherapy, Adv Sci (Weinh). 11 (3) (2024) e2305217, https://doi.org/10.1002/advs.202305217.

[30] K.J. Rambhia, P.X. Ma, Controlled drug release for tissue engineering, J. Control. Release 219 (2015 Dec 10) 119–128, https://doi.org/10.1016/j.jconrel.2015.08.049 (Epub 2015 Aug 29).

[31] A. Tampieri, A. Ruffini, A. Ballardini, M. Montesi, S. Panseri, F. Salamanna, M. Fini, S. Sprio, Heterogeneous chemistry in the 3-D state: an original approach to generate bioactive, mechanically-competent bone scaffolds, Biomater. Sci. 7 (2018) 307–321, https://doi.org/10.1039/c8bm01145a.

[32] E. Kon, F. Salamanna, G. Filardo, B. Di Matteo, N. Shabshin, J. Shani, M. Fini, F. Perdisa, A. Parrilli, S. Sprio, et al., Bone Regeneration in Load-Bearing Segmental Defects, Guided by Biomorphic, Hierarchically Structured Apatitic Scaffold, Front. Bioeng. Biotechnol. 9 (2021) 734486, https://doi.org/10.3389/fbioe.2021.734486.

[33] S. Sprio, S. Panseri, M. Montesi, M. Dapporto, A. Ruffini, S.M. Dozio, R. Cavuoto, D. Misseroni, M. Paggi, D. Bigoni, et al., Hierarchical porosity inherited by natural sources affects the mechanical and biological behaviour of bone scaffolds, J. Eur. Ceram. Soc. 40 (2020) 1717–1727, https://doi.org/10.1016/j.jeurceramsoc.2019.11.015.

[34] D. Bigoni, R. Cavuoto, D. Misseroni, M. Paggi, A. Ruffini, S. Sprio, A. Tampieri, Ceramics with the signature of wood: a mechanical insight, Mater. Today Bio 5 (2020) 100032, https://doi.org/10.1016/j.mtbio.2019.100032.

[35] Y. Du, J.L. Guo, J. Wang, A.G. Mikos, S. Zhang, Hierarchically designed bone scaffolds: From internal cues to external stimuli, Biomaterials 218 (2019) 119334, https://doi.org/10.1016/j.biomaterials.2019.119334.

[36] S. Sprio, A. Ruffini, A. Tampieri, Biomorphic transformations: A leap forward in getting nanostructured 3-D bioceramics, Front. Chem. 9 (2021) 728907, https://doi.org/10.3389/fchem.2021.728907.

[37] F. Salamanna, A. De Luca, F. Vandenbulcke, B. Di Matteo, E. Kon, A. Grassi, A. Ballardini, G. Morozzi, L. Raimondi, D. Bellavia, et al., Preliminary osteogenic and antibacterial investigations of wood derived antibiotic-loaded bone substitute for the treatment of infected bone defects, Front. Bioeng. Biotechnol. 12 (2024) 1412584, https://doi.org/10.3389/fbioe.2024.1412584.

[38] L. Mercatali, F. La Manna, G. Miserocchi, C. Liverani, A. De Vita, C. Spadazzi, A. Bongiovanni, F. Recine, D. Amadori, M. Ghetti, et al., Tumor-stroma crosstalk in bone tissue: The osteoclastogenic potential of a breast cancer cell line in a Co-culture system and the role of EGFR inhibition, Int. J. Mol. Sci. 18 (2017) 1655, https://doi.org/10.3390/ijms18081655.

[39] E. Veronesi, A. Murgia, A. Caselli, G. Grisendi, M.S. Piccinno, V. Rasini, R. Giordano, T. Montemurro, P. Bourin, L. Sensebé, et al., Transportation conditions for prompt use of ex vivo expanded and freshly harvested clinical-grade bone marrow mesenchymal stromal/stem cells for bone regeneration, Tissue Eng. Part C Methods 20 (2014) 239–251, https://doi.org/10.1089/ten.TEC.2013.0250.

[40] A.A. Dussault, M. Pouliot, Rapid and simple comparison of messenger RNA levels using real-time PCR, Biol. Proced. Online 8 (2006) 1–10, https://doi.org/10.1251/bpo114.

[41] M. Cortesi, C. Liverani, L. Mercatali, T. Ibrahim, E. Giordano, An in-silico study of cancer cell survival and spatial distribution within a 3D microenvironment, Sci. Rep. 10 (2020) 12976, https://doi.org/10.1038/s41598-020-69862-7.

[42] M. Cortesi, D. Liu, C. Yee, D.J. Marsh, C.E. Ford, A comparative analysis of 2D and 3D experimental data for the identification of the parameters of computational models, Sci. Rep. 13 (2023) 15769, https://doi.org/10.1038/s41598-023-42486-3.

[43] M. Cortesi, E. Giordano, Driving cell response through deep learning, a study in simulated 3D cell cultures, Heliyon 10 (2024) e29395, https://doi.org/10.1016/j.heliyon.2024.e29395.

[44] A. Ruffini, S. Sprio, A. Tampieri, Study of the hydrothermal transformation of wood-derived calcium carbonate into 3D hierarchically organized hydroxyapatite, Chem. Eng. J. 217 (2013) 150–158, https://doi.org/10.1016/j.cej.2012.11.107.

[45] D.J. Mooney, D.F. Baldwin, N.P. Suh, J.P. Vacanti, R. Langer, Novel approach to fabricate porous sponges of poly(D,L-lactic-co-glycolic acid) without the use of organic solvents, Biomaterials 17 (1996) 1417–1422, https://doi.org/10.1016/0142-9612(96)87284-x.
[46] K.R. Schultz, A. Carroll, N.A. Heerema, W.P. Bowman, A. Aledo, W.B. Slayton, H. Sather, M. Devidas, H.W. Zheng, S.M. Davies, et al., Long-term follow-up of imatinib in pediatric Philadelphia chromosome-positive acute lymphoblastic leukemia: Children's Oncology Group study AALL0031, Leukemia 28 (2014) 1467–1471, https://doi.org/10.1038/leu.2014.30.
[47] A. Bigham, A.H. Aghajanian, S. Behzadzadeh, Z. Sokhani, S. Shojaei, Y. Kaviani, S. A. Hassanzadeh-Tabrizi, Nanostructured magnetic Mg2SiO4-CoFe2O4 composite scaffold with multiple capabilities for bone tissue regeneration, Mater. Sci. Eng. 99 (2019) 83–95, https://doi.org/10.1016/j.msec.2019.01.096.
[48] A. Abdal-hay, F.A. Sheikh, J.K. Lim, Air jet spinning of hydroxyapatite/poly(lactic acid) hybrid nanocomposite membrane mats for bone tissue engineering, Colloids Surf. B: Biointerfaces 102 (2013) 635–643, https://doi.org/10.1016/j.colsurfb.2012.09.017.
[49] A. Bigham, A.H. Aghajanian, A. Saudi, M. Rafienia, Hierarchical porous Mg2SiO4-CoFe2O4 nanomagnetic scaffold for bone cancer therapy and regeneration: Surface modification and in vitro studies, Mater. Sci. Eng. 109 (2020) 110579, https://doi.org/10.1016/j.msec.2019.110579.
[50] K. Koto, H. Murata, Y. Sawai, E. Ashihara, M. Horii, T. Kubo, Cytotoxic effects of zoledronic acid-loaded hydroxyapatite and bone cement in malignant tumors, Oncol. Lett. 14 (2017) 1648–1656, https://doi.org/10.3892/ol.2017.6355.
[51] J.S. Gogia, J.P. Meehan, P.E. Di Cesare, A.A. Jamali, Local antibiotic therapy in osteomyelitis, Semin. Plast. Surg. 23 (2009) 100–107, https://doi.org/10.1055/s-0029-1214162.
[52] E. Oledzka, D. Pachowska, K. Orłowska, J. Kolmas, A. Drobniewska, R. Figat, M. Sobczak, Pamidronate-conjugated biodegradable branched copolyester carriers: synthesis and characterization, Molecules 22 (2017) 1063, https://doi.org/10.3390/molecules22071063.
[53] M.A. Lopez-Heredia, G.J. Kamphuis, P.C. Thüne, F.C. Öner, J.A. Jansen, X. F. Walboomers, An injectable calcium phosphate cement for the local delivery of paclitaxel to bone, Biomaterials 32 (2011) 5411–5416, https://doi.org/10.1016/j.biomaterials.2011.04.010.
[54] P. Ahangar, E. Akoury, A.S. Ramirez Garcia Luna, A. Nour, M.H. Weber, D. H. Rosenzweig, Nanoporous 3D-printed scaffolds for local doxorubicin delivery in bone metastases secondary to prostate cancer, Materials (Basel) 11 (2018) 1485, https://doi.org/10.3390/ma11091485.
[55] H. Liu, E.B. Slamovich, T.J. Webster, Less harmful acidic degradation of poly (lacticco-glycolic acid) bone tissue engineering scaffolds through titania nanoparticle addition, Int. J. Nanomedicine 1 (2006) 541–545, https://doi.org/10.2147/nano.2006.1.4.541.
[56] A. Tampieri, S. Sprio, A. Ruffini, G. Celotti, I.G. Lesci, N. Roveri, From wood to bone: multi-step process to convert wood hierarchical structures into biomimetic hydroxyapatite scaffolds for bone tissue engineering, J. Mater. Chem. 19 (2009) 4973–4980, https://doi.org/10.1039/b900333a.
[57] C. Pitsilos, P.V. Giannoudis, Distal femoral bone defect treatment using an engineered hydroxyapatite cylinder scaffold made from rattan wood, BMJ Case Rep. 18 (2025) e264131, https://doi.org/10.1136/bcr-2024-264131.
[58] P.V. Giannoudis, P. Andrzejwski, G. Chloros, E.M.A. Hensor, Safety and performance of a novel synthetic biomimetic scaffold for iliac crest defect reconstruction during surgical treatment of pelvic girdle pain: a first-in-human trial, Br. Med. Bull. 153 (2025) ldae023, https://doi.org/10.1093/bmb/ldae023.
[59] V. Alt, N. Walter, M. Rupp, T. Begué, M. Plecko, Bone defect filling with a novel rattan-wood based not-sintered hydroxyapatite and beta-tricalcium phosphate material (b.Bone™) after tricortical bone graft harvesting - a consecutive clinical case series of 9 patients, Trauma Case Rep. 44 (2023) 100805, https://doi.org/10.1016/j.tcr.2023.100805.
[60] C. Moreau-Bachelard, M. Robert, C. Gourmelon, E. Bourbouloux, A. Patsouris, J. S. Frenel, M. Campone, Evaluating everolimus for the treatment of breast cancer. Evaluating everolimus for the treatment of breast cancer, Expert. Opin. Pharmacother. 24 (2023) 1105–1111, https://doi.org/10.1080/14656566.2023.2214677.
[61] T. Powles, L. Albiges, A. Bex, E. Comperat, V. Grünwald, R. Kanesvaran, H. Kitamura, R. McKay, C. Porta, G. Procopio, et al., Renal cell carcinoma: ESMO Clinical Practice Guideline for diagnosis, treatment and follow-up, Ann. Oncol. 35 (2024) 692–706, https://doi.org/10.1016/j.annonc.2024.05.537.
[62] R. Muff, S.M. Botter, K. Husmann, J. Tchinda, P. Selvam, F. Seeli-Maduz, B. Fuchs, Explant culture of sarcoma patients' tissue, Lab. Investig. 96 (2016) 752–762, https://doi.org/10.1038/labinvest.2016.49.
[63] M. Rodolfo, V. Huber, M. Cossa, G. Gallino, B.E. Leone, V. Vallacchi, L. Rivoltini, E. Vergani, 3D tumor explant as a novel platform to investigate therapeutic pathways and predictive biomarkers in cancer patients, Front. Immunol. 13 (2022) 1068091, https://doi.org/10.3389/fimmu.2022.1068091.
[64] F. Pantano, E. Rossi, M. Iuliani, A. Facchinetti, S. Simonetti, G. Ribelli, A. Zoccoli, B. Vincenzi, G. Tonini, R. Zamarchi, et al., Dynamic changes of receptor activator of nuclear factor-κB expression in circulating tumor cells during denosumab predict treatment effectiveness in metastatic breast cancer, Sci. Rep. 10 (2020) 1288, https://doi.org/10.1038/s41598-020-58339-2.

Glossary

BC breast carcinoma:
BM bone metastases:
BTA bone-targeted agents:
ccRCC clear-cell renal carcinoma cell line:
CPC calcium phosphate cement:
DFS disease-free survival:
EVE everolimus:
FBS fetal bovine serum:
Obs osteoblasts:
Ocs osteoclasts:
PBMC peripheral blood mononuclear cell:
PDE Patient derived explant:
RCC renal cell:
SEM scanning electron microscopy:
TNBC triple negative BC cell:
TRAP tartrate resistant acid phosphatase: